



# Decentralized optimal control of Connected Automated Vehicles at signal-free intersections including comfort-constrained turns and safety guarantees<sup>☆</sup>

Yue Zhang, Christos G. Cassandras<sup>\*</sup>

Division of Systems Engineering and Center for Information and Systems Engineering, Boston University, Boston, MA 02215, USA

## ARTICLE INFO

### Article history:

Received 29 January 2019  
Received in revised form 15 August 2019  
Accepted 16 August 2019  
Available online 5 September 2019

## ABSTRACT

We extend earlier work for optimally controlling Connected Automated Vehicles (CAVs) crossing a signal-free intersection by including all possible turns taken so as to optimize a passenger comfort metric along with energy and travel time minimization. We show that it is possible to achieve this goal in a decentralized manner with each CAV solving an optimal control problem, and derive explicit solutions that guarantee collision avoidance and safe distance constraints within a control zone. We investigate the associated tradeoffs between minimizing energy and vehicle travel time, as well as the passenger comfort metric and include extensive simulations to illustrate this framework.

© 2019 Elsevier Ltd. All rights reserved.

## 1. Introduction

Intersections in transportation systems are one of the major traffic control challenges as they account for a large part of accidents and of overall road congestion. As documented in Schrank, Eisele, Lomax, and Bak (2015), in 2014, traffic congestion caused vehicles in urban areas to spend 6.9 billion extra hours on the road at a cost of an extra 3.1 billion gallons of fuel, resulting in a total cost estimated at \$160 billion. From a control and optimization standpoint, the goal is to develop efficient traffic management methods so as to reduce congestion and increase safety with minimal impact on the existing infrastructure. This is typically accomplished through tighter spacing of vehicles (Malikopoulos & Aguilar, 2013; Margiotta & Snyder, 2011) which can alleviate congestion, reduce energy use and emissions, and improve safety under proper control. Forming “platoons” of vehicles is a popular system-level approach that gained momentum in the 1990s (Rajamani, Tan, Law, & Zhang, 2000; Shladover, Desoer, Hedrick, Tomizuka, Walrand, Zhang, McMahon, Peng, Sheikholeslam, & McKeown, 1991). More recently, a

study in Tachet, Santi, Sobolevsky, Reyes-Castro, Frazzoli, Helbing, and Ratti (2016) indicated that transitioning from intersections with traffic lights to autonomous ones has the potential of doubling capacity and reducing delays.

To date, traffic light control is the prevailing method for coordinating conflicting traffic flows and ensure road safety in urban areas. Recent technological developments include designing adaptive traffic light control systems that can dynamically adjust the signal timing to various context, e.g., Fleck, Cassandras, and Geng (2016) and references therein. However, in addition to the obvious infrastructure cost of traffic lights, the efficiency and safety offered by such signaling methods is limited, thus motivating research efforts to explore new approaches capable of enabling smoother traffic flow while ensuring safety.

Connected Automated Vehicles (CAVs), also referred to as autonomous or self-driving vehicles, provide the most intriguing opportunity for better traffic conditions in a transportation network and for improving traffic flow. CAVs can assist drivers in making better operating decisions or they can do so in a fully automated way so as to improve safety and reduce pollution, energy consumption, and travel delays. According to SAE International's definition (SAE International, 2016), there are five autonomy levels, from level 1, where an Advanced Driver Assistance System (ADAS) is embedded to assist the human driver, to level 5 where a fully automated driving system is in place requiring no human intervention. The CAVs in our paper are assumed to be at least at level 4 (where control can be relinquished back to the driver under certain circumstances). CAVs can also use different technologies to communicate with other elements in the traffic system, e.g., vehicle-to-vehicle (V2V) or vehicle-to-infrastructure (V2I). The CAVs in our paper are assumed to be

<sup>☆</sup> Supported in part by NSF, USA under grants ECCS-1509084, DMS-1664644, and CNS-1645681, by AFOSR, USA under grant FA9550-19-1-0158, by ARPA-E's NEXTCAR program under grant DE-AR0000796 and by the MathWorks. The material in this paper was partially presented at the 56th IEEE Conference on Decision and Control, December 12–15, 2017, Melbourne, Australia. This paper was recommended for publication in revised form by Associate Editor Antonella Ferrara under the direction of Editor Thomas Parisini.

<sup>\*</sup> Corresponding author.

E-mail addresses: [joyce@bu.edu](mailto:joyce@bu.edu) (Y. Zhang), [cgc@bu.edu](mailto:cgc@bu.edu) (C.G. Cassandras).

capable of communicating to everything (V2X) without errors and delays. We note, however, that the decentralized nature of our controller limits the information required by each CAV from other CAVs, thus reducing the communication load.

One of the very early efforts in this direction was proposed in Athans (1969) and Levine and Athans (1966) where the merging problem was formulated as a linear optimal regulator to control a single string of vehicles. The key features of an automated intelligent vehicle-highway system (IVHS) and a related control system architecture are discussed in Varaiya (1993). More recently, several research efforts have been reported in the literature for CAV coordination at intersections. Dresner and Stone (2004) proposed a reservation-based scheme for centralized automated vehicle intersection management while no turns are allowed. Since then, numerous research efforts have explored safe and efficient control strategies, e.g., de La Fortelle (2010), Dresner and Stone (2008) and Huang, Sadek, and Zhao (2012). Several efforts have focused on minimizing vehicle travel time under collision-avoidance constraints (Lee & Park, 2012; Li & Wang, 2006; Miculescu & Karaman, 2014; Yan, Dridi, & El Moudni, 2009; Zhu & Ukkusuri, 2015; Zohdy, Kamalanathsharma, & Rakha, 2012). Zohdy et al. (2012) presented an approach based on Cooperative Adaptive Cruise Control (CACC) for minimizing intersection delay and hence maximizing the throughput. Lee and Park (2012) considered minimizing the overlap between vehicle positions. Miculescu and Karaman (2014) have studied intersections as polling systems and determined a sequence of times assigned to vehicles on each road which provides provable guarantees on safety and expected wait time. Reducing energy consumption is another desired objective which has been considered in recent literature (Gilbert, 1976; Hellström, Åslund, & Nielsen, 2010; Hooker, 1988; Li, Peng, Li, & Wang, 2012). Hellström et al. (2010) proposed an energy-optimal control algorithm for heavy diesel trucks by utilizing road topography information. Based on Vehicle-to-Vehicle (V2V) communication, a minimum energy control strategy is investigated in car-following scenarios in Li et al. (2012). A detailed discussion of recent advances in this area can be found in Rios-Torres and Malikopoulos (2017).

Our earlier work (Malikopoulos, Cassandras, & Zhang, 2018; Zhang, Malikopoulos, & Cassandras, 2016) established a decentralized optimal control framework for coordinating on line a continuous flow of CAVs crossing an urban intersection without using explicit traffic signaling, assuming no left and right turns are allowed. For each CAV, an energy minimization optimal control problem is formulated where the time to cross the intersection is first determined through a throughput maximization problem. We solved this problem for each CAV entering a specified *Control Zone* (CZ) so that the acceleration/deceleration of the CAV is controlled until it reaches a *Merging Zone* (MZ) where the potential of lateral collisions exists. To ensure safety, we required CAVs to have a constant speed through the MZ while also maintaining a safe distance between them to avoid rear-end collisions. The presence of hard safety constraints makes it challenging to ensure the existence of a feasible solution to each such decentralized problem. Therefore, we also established in Zhang et al. (2016) the conditions under which such feasible solutions exist and showed that they can be enforced through an appropriately designed Feasibility Enforcement Zone (FEZ) that precedes the CZ in Zhang, Cassandras, and Malikopoulos (2017).

The inclusion of left and right turns in this framework creates significant complications. Aside from the added complexity of ensuring collision avoidance, we can no longer expect each CAV to maintain a constant speed in the MZ. Instead, we must allow a CAV to vary its speed depending on the turn. In addition, passenger comfort in taking such turns becomes an essential component of an automated trajectory design. The problem of coordinating

CAVs at intersections including left and right turns has been addressed by Kim and Kumar (2014) based on an approach using Model Predictive Control (MPC) to achieve system-wide safety and liveness of intersection-crossing traffic. Dresner and Stone in Dresner and Stone (2005) considered scenarios that allowed left and right turns using a reservation-based scheme together with a communication protocol which may involve a stop sign and traffic lights.

The contribution of this paper consists of extending the optimal control framework in Zhang et al. (2016). First, unlike the approach in Zhang et al. (2016) where we first solved a throughput maximization problem to determine a CAV's travel time and then an energy minimization problem for each CAV, here we formulate a problem in which a CAV seeks to *jointly minimize* both its travel time through the CZ and its energy consumption. This allows us to readily quantify the tradeoff between these two criteria. Second, we formulate and solve a subsequent optimal control problem for each CAV crossing the MZ in which we allow it to vary its speed inside the MZ and include a passenger comfort metric when a turn is taken. The ability to decentralize the optimal control in Zhang et al. (2016) rests on showing that each CAV needs only information from the CAV which is physically ahead of it and the one immediately preceding it in entering the CZ. The presence of turns complicates this simple coordination structure; however, we are still able to show that each CAV needs only information from a small set of well-defined CAVs among those preceding it (but not necessarily immediately preceding it) in entering the CZ. We also derive explicit solutions for the two optimal control problems, through the CZ and then the MZ, including the possibility of safety, state and control constraints becoming active. Our analysis includes the derivation of properties characterizing an optimal control solution, such as the continuity of the optimal control when an unconstrained optimal trajectory arc is followed by one with an active constraint, and it allows us to determine whether an optimal control solution for each CAV is feasible at the time it enters the CZ.

The paper is structured as follows. In Section 2, we review the model in Zhang et al. (2016) and extend it to include left and right turns. In Section 3, we derive the conditions that guarantee safety for each CAV in terms of its time to reach the MZ constrained by those of CAVs preceding it in the CZ. In Section 4, we formulate a decentralized optimal control problem for each CAV that jointly minimizes its travel time and energy consumption, prove structural properties of optimal trajectories, and derive an explicit solution for it. In Section 5, we formulate and solve another optimization problem with the objective of jointly minimizing a passenger comfort metric inside the MZ and its energy consumption. Simulation results are given in Section 6 where the time-energy tradeoff is illustrated, as well as the comfort-energy tradeoff.

## 2. The intersection model

We begin with a brief review of the model introduced in Zhang et al. (2016) and fully developed in Malikopoulos et al. (2018). We consider an intersection (Fig. 1) where the region at its center, assumed to be a square of side  $S$ , is called *Merging Zone* (MZ) and defines the area of potential lateral CAV collisions. The intersection has a *Control Zone* (CZ) and the road segment from the CZ entry to the CZ exit (i.e., the MZ entry) is referred to as a CZ segment. The length of each CZ segment is  $L > S$  and it is assumed to be the same for all entry points to a given CZ. Extensions to asymmetric CZ segments are possible and considered in Zhang and Cassandras (2018a).

We assume the existence of a “coordinator” whose task is to handle the information exchanges between CAVs, while each CAV maintains its own control autonomy. Let  $N(t) \in \mathbb{N}$  be the

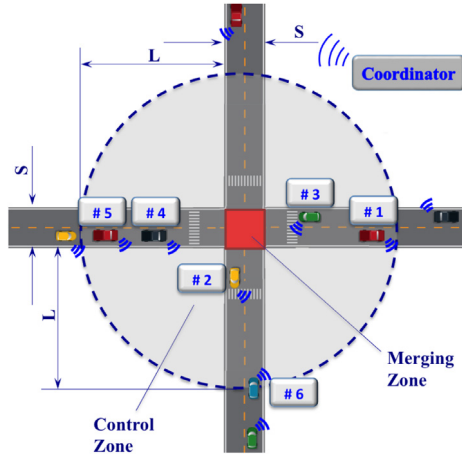


Fig. 1. Connected automated vehicles crossing an urban intersection.

cumulative number of CAVs which have entered the CZ by time  $t$  and formed a queue that designates the crossing sequence in which these CAVs will enter the MZ. There is a number of ways to manage such a queue. In Zhang et al. (2016) a strict First-In-First-Out (FIFO) crossing sequence is assumed, that is, when a CAV reaches the CZ, the coordinator assigns it an integer value  $i = N(t) + 1$ . This can be relaxed as in Zhang and Cassandras (2018a) to allow for dynamically resequencing CAVs as each new one arrives, hence maximizing throughput. If two or more CAVs enter a CZ at the same time, then the corresponding coordinator selects randomly the first one to be assigned the value  $N(t) + 1$ .

For simplicity, we assume that each CAV is governed by second order dynamics:

$$\dot{p}_i = v_i(t), \quad p_i(t_i^0) = 0; \quad \dot{v}_i = u_i(t), \quad v_i(t_i^0) \text{ given} \quad (1)$$

where  $p_i(t) \in \mathcal{P}_i$ ,  $v_i(t) \in \mathcal{V}_i$ , and  $u_i(t) \in \mathcal{U}_i$  denote the position, i.e., travel distance since the entry of the CZ, speed and acceleration/deceleration (control input) of each CAV  $i$ . The sets  $\mathcal{P}_i$ ,  $\mathcal{V}_i$  and  $\mathcal{U}_i$  are complete and totally bounded subsets of  $\mathbb{R}$ . These dynamics are in force over an interval  $[t_i^0, t_i^f]$ , where  $t_i^0$  and  $t_i^f$  are the times that the vehicle  $i$  enters the CZ and exits the MZ respectively. To ensure that the control input and vehicle speed are within a given admissible range, the following constraints are imposed:

$$u_{i,\min} \leq u_i(t) \leq u_{i,\max}, \quad \text{and} \quad 0 \leq v_{\min} \leq v_i(t) \leq v_{\max}, \quad \forall t \in [t_i^0, t_i^f]. \quad (2)$$

To ensure the absence of any rear-end collision throughout the CZ, we impose the *rear-end safety* constraint

$$s_i(t) = p_k(t) - p_i(t) \geq \delta, \quad \forall t \in [t_i^0, t_i^f] \quad (3)$$

where  $k$  is the CAV physically ahead of  $i$  and  $\delta$  is the *minimal safe following distance* allowable. An alternative safety constraint often used is to maintain a safe headway (Rajamani et al., 2000), i.e., a time gap that is a function of speed. However, since we consider urban intersections, the average speed does not exhibit significant variations and we can translate the allowable headway to a safe inter-vehicle distance (replacing (3) by a headway constraint is still possible at the expense of complicating the explicit solutions to the optimal control problems we will consider in the sequel).

In this modeling framework, we assume that (i) CAVs follow the crossing sequence established by the coordinator and that **no overtaking, reversing directions, or lane-changing are allowed**, (ii) each vehicle has proximity sensors and can observe and/or estimate local information that can be shared with other vehicles (this is already redundant in most commercially available modern

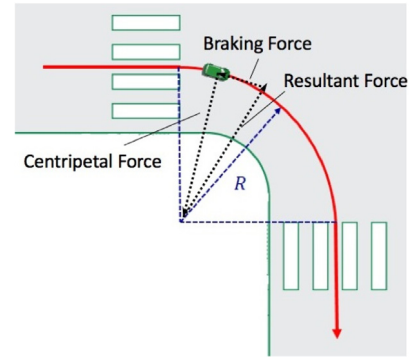


Fig. 2. Vehicle making a turn.

vehicles), (iii) the decision of each CAV on whether a turn needs to be made at the MZ is known upon its entry in the CZ and remains unchanged, and (iv) for each CAV, the speed constraints in (2) and the rear-end safety constraint in (3) are not active at  $t_i^0$ . If this last assumption is violated, any optimal control solution is obviously infeasible and we must resort to control actions that simply attempt to satisfy these constraints as promptly as possible; alternatively, we may impose a Feasibility Enforcement Zone (FEZ) that precedes the CZ as described in Zhang et al. (2017).

Finally, we make the following simplifying assumption:

**Assumption 1.** For each CAV  $i$  exiting the MZ, its speed remains constant for at least a distance of length  $\delta$ .

This assumption is reasonable since there is no compelling reason for vehicles to accelerate or decelerate right after they exit the MZ unless an imminent safety issue is involved.

## 2.1. Modeling turns

The inclusion of left and right turns needs special attention in the context of safety as well in ensuring passenger comfort. As a vehicle turns, it is affected simultaneously by two forces: the braking force and the centripetal force (see Fig. 2). Note that the centripetal force is provided by the friction force, which depends on the speed of the vehicle. Hence, to ensure safety, vehicles need to slow down while making turns. The smaller the turning radius is, the lower the speed needs to be. On the other hand, to minimize passenger discomfort, vehicles need to maintain a steady movement, i.e., avoid any abrupt change in the braking force. In other words, we need to minimize the change in acceleration (i.e., the *jerk*).

Let  $d_i$  denote the decision of vehicle  $i$  on whether a turn is to be made at the MZ, where  $d_i = 0$  indicates a left turn,  $d_i = 1$  indicates going straight and  $d_i = 2$  indicates a right turn. Letting  $S_L$  denote the length of the left turn trajectory and  $S_R$  the length of the right turn trajectory, we assume that  $S_R < S < S_L$  holds. The speed for which an intersection curve is designed depends on an assigned speed limit, the type of intersection, and the traffic volume (Aashto, 2001). Generally, the “desirable time”  $\Delta_i$  that a vehicle needs to make a turn at an intersection (Aashto, 2001) is given by

$$\Delta_i = \begin{cases} \frac{R_i}{\sqrt{15R_i(0.01E + F)}}, & \text{if } d_i = 0, 2, \\ \Delta_i^1, & \text{if } d_i = 1, \end{cases} \quad (4)$$

where  $R_i$  is the centerline turning radius (see Fig. 2);  $E$  is the super-elevation, which is zero in urban conditions;  $F$  is the side

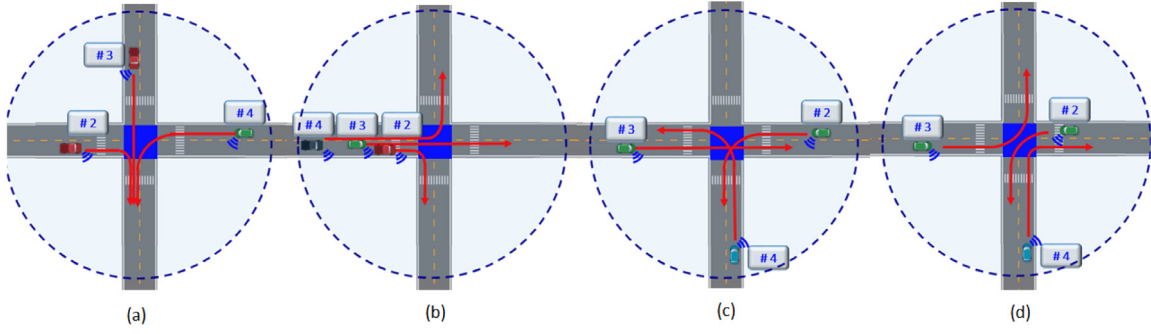


Fig. 3. Illustration of different subsets of  $\mathcal{Q}^z(t)$ : (a) subset  $\mathcal{E}(t)$ ; (b) subset  $\mathcal{S}(t)$ ; (c) subset  $\mathcal{L}(t)$ ; (d) subset  $\mathcal{O}(t)$ .

friction factor; and  $\Delta_i^1$  is the time for CAV  $i$  going straight. Therefore, the time  $t_i^m$  when CAV  $i$  enters the MZ is directly related to the time  $t_i^f$  that the vehicle exits the MZ through  $\Delta_i$ :

$$t_i^f = t_i^m + \Delta_i. \quad (5)$$

Note that  $\Delta_i$  is different for left and right turns since the associated turning radii  $R_i$  are different.

## 2.2. Relative location sets

When a CAV enters the CZ and is assigned a unique index  $i = N(t) + 1$  by the coordinator, it is also assigned to one and only one of four subsets  $\{\mathcal{E}_i(t), \mathcal{S}_i(t), \mathcal{L}_i(t), \mathcal{O}_i(t)\}$  which capture its position relative to CAVs  $j < i$ . These subsets are considerably different than those in Zhang et al. (2016) due to the presence of turns and are defined as follows:

(1)  $\mathcal{E}_i(t)$  contains all vehicles  $j < i$  that can cause a rear-end collision with  $i$  at the end of the MZ. For example, in Fig. 3(a),  $\mathcal{E}_3(t)$  contains vehicle #2 as it may cause a rear-end collision with vehicle #3 at the end of the MZ, and  $\mathcal{E}_4(t)$  contains vehicle #3 as it may cause a rear-end collision with vehicle #4 at the end of the MZ.

(2)  $\mathcal{S}_i(t)$  contains all vehicles  $j < i$  traveling on the same lane that can cause rear-end collision with  $i$  at the beginning of the MZ. For example, in Fig. 3(b),  $\mathcal{S}_3(t)$  contains vehicle #2 as it may cause a rear-end collision with vehicle #3 at the beginning of the MZ, and  $\mathcal{S}_4(t)$  contains vehicle #3 as it may cause a rear-end collision with vehicle #4 at the beginning of the MZ. Note that if CAVs  $j$  and  $i, j < i$  travel on the same lane and in the same direction, we have  $j \in \mathcal{E}_i(t)$ ; since  $j$  belongs to one and only one of these subsets, we cannot have  $j \in \mathcal{S}_i(t)$ .

(3)  $\mathcal{L}_i(t)$  contains all vehicles  $j < i$  traveling on different lanes and towards different lanes that can cause lateral collision with  $i$  inside the MZ. For example, in Fig. 3(c),  $\mathcal{L}_3(t)$  contains vehicle #2 as it may cause a lateral collision with vehicle #3 inside the MZ, and  $\mathcal{L}_4(t)$  contains vehicle #3 as it may cause a lateral collision with vehicle #4 inside the MZ.

(4)  $\mathcal{O}_i(t)$  contains all vehicles  $j < i$  traveling on different lanes and towards different directions that cannot cause any lateral collision with  $i$  at the MZ. For example, in Fig. 3(d),  $\mathcal{O}_3(t)$  contains vehicle #2 since it cannot cause any collision with vehicle #3, and  $\mathcal{O}_4(t)$  contains vehicle #3 since it cannot cause any collision with vehicle #4.

## 2.3. Merging zone safety constraints

As in Zhang et al. (2016), we consider a First-In-First-Out (FIFO) queue by imposing the following condition:

$$t_i^f \geq t_{i-1}^f, \quad i > 1. \quad (6)$$

However, as already mentioned, this FIFO structure may be relaxed by dynamically resequencing CAVs as each new one arrives (Zhang & Cassandras, 2018a) aiming to maximize throughput and subsequently re-solving each decentralized CAV problem. As we will see, this is made possible by the relatively modest computational cost of solving such problems.

A lateral collision involving CAV  $i$  may occur only if some CAV  $j \neq i$  belongs to  $\mathcal{L}_i(t)$ . This leads to the following definition:

**Definition 1.** For each CAV  $i \in \mathcal{N}(t)$ , the set  $\Gamma_i$  that includes all time instants when a lateral collision involving CAV  $i$  is possible:  $\Gamma_i \triangleq \{t \mid t \in [t_i^m, t_i^f]\}$ .

Consequently, to avoid a lateral collision for any two vehicles  $i, j \in \mathcal{N}(t)$  on different roads, the following constraint should hold:

$$\Gamma_i \cap \Gamma_j = \emptyset, \quad \forall t \in [t_i^m, t_i^f], \quad j \in \mathcal{L}_i(t). \quad (7)$$

In earlier work (Zhang et al., 2016), the speed in the MZ was considered to be constant, a condition made possible by the fact that, in the absence of turns, all CAVs have the same trajectory within the MZ. Thus,  $t_i^m > t_{i-1}^m$  could be implicitly ensured by  $t_i^f > t_{i-1}^f$ . Since this is no longer the case, i.e., speeds and position trajectories in the MZ may be different for CAVs with different driving directions (e.g., CAV  $i$  may turn left while CAV  $i - 1$  is going straight), the condition  $t_i^f \geq t_{i-1}^f$  does not imply  $t_i^m \geq t_{i-1}^m$ . This becomes an issue only when  $i$  and  $i - 1$  are traveling on the same lane. We shall henceforth reserve the symbol  $k$  ( $k < i$ ) to denote the index of the CAV physically located ahead of  $i$ . Then, for CAVs  $i$  and  $k$  we impose the following constraint:

$$t_i^m > t_k^m, \quad i > k \geq 1, \quad (8)$$

to avoid any rear-end collision at the beginning of the MZ.

## 2.4. Terminal conditions

We now turn our attention to the terminal conditions that must be enforced on each CAV  $i$  at times  $t_i^m$  and  $t_i^f$  when it enters and exits the MZ respectively. The safety requirements discussed above imply constraints on these times that depend on the relative location sets of  $i$  as explained next.

(1) Let  $e = \max_j \{j \in \mathcal{E}_i(t)\}$ . In this case, CAV  $e$  is the vehicle immediately ahead of CAV  $i$  in the FIFO queue that may cause a rear-end collision with  $i$  at the end of the MZ. To avoid such a rear-end collision,  $e$  and  $i$  should maintain the minimal safe distance  $\delta$  defined in (3) by the time  $i$  exits the MZ. Since, by Assumption 1, each CAV maintains a constant speed after the MZ exit for at least a distance  $\delta$ , we set

$$t_i^f \geq t_e^f + \frac{\delta}{v_e} \quad (9)$$



where  $t_e^f$  and  $t_i^f$  are the times that CAVs  $e$  and  $i$  exit the MZ respectively, and  $v_e^f$  is the speed of CAV  $e$  at the exit of the MZ. It is easy to see that if the only objective for  $i$  is to minimize its travel time, then it should set  $t_i^f = t_e^f + \delta/v_e^f$ . In general, however, as we will see when setting up each CAV's decentralized optimal control problem in Section 4, (9) in conjunction with (5) provides only a lower bound constraint on  $t_i^m$  for this problem:

$$t_i^m \geq t_e^f + \frac{\delta}{v_e^f} - \Delta_i \quad (10)$$

Unlike our earlier work (Zhang et al., 2016) where we considered a constant speed for all CAVs inside the MZ, the inclusion of **left and right turns forces us to vary the speed**  $v_i(t)$  for  $t \in [t_i^m, t_i^f]$ . The actual values of  $v_i(t)$ ,  $t \in [t_i^m, t_i^f]$ , are determined by the solution of the optimal control problem we will define in Section 5 so as to take a passenger comfort metric into consideration. For this problem,  $t_i^m$  is the initial time which is obtained from the decentralized optimal control problem over  $[t_i^0, t_i^m]$  in Section 4.

(2) Let  $s = \max_j \{j \in S_i(t)\}$ . In this case, CAV  $s$  is the vehicle immediately ahead of CAV  $i$  in the FIFO queue such that it may cause a rear-end collision at the beginning of the MZ. To guarantee the rear-end collision constraint does not become active we set

$$t_i^m \geq t_s^m + \Delta_s^\delta, \quad (11)$$

where, in view of (4),

$$\Delta_s^\delta = \begin{cases} \frac{\delta}{\sqrt{15R_i(0.01E + F)}}, & \text{if } d_s = 0, 2, \\ \Delta_s^{1\delta}, & \text{if } d_s = 1. \end{cases} \quad (12)$$

is the time vehicle  $s$  needs to travel a distance  $\delta$  inside the MZ, where  $\Delta_s^{1\delta}$  is the time for CAV  $s$  traveling a distance  $\delta$  if it goes straight. The time  $t_i^f$  when CAV  $i$  will be exiting the MZ is given by (5) and, using (11), we get  $t_i^f \geq t_s^m + \Delta_s^\delta + \Delta_i$ . However, if  $s$  makes a left turn and  $i$  makes a right turn, since  $S_L > S_R$ , we may have  $t_i^f < t_s^f$ , which violates (6). In that case, we must set  $t_i^f \geq t_s^f$ . This situation arises whenever the time to cover the trajectory of  $s$  through the MZ is longer than that of  $i$ . Combining these two cases, it follows that

$$t_i^f \geq \max\{t_s^m + \Delta_s^\delta + \Delta_i, t_s^f\} \quad (13)$$

and, from (5),  $t_i^m$  is constrained so that

$$t_i^m \geq \max\{t_s^m + \Delta_s^\delta, t_s^f - \Delta_i\}$$

(3) Let  $l = \max_j \{j \in \mathcal{L}_i(t)\}$ . In this case, CAV  $l$  is the vehicle immediately ahead of CAV  $i$  in the FIFO queue such that it may cause a lateral collision inside the MZ. We constrain the MZ to contain only either CAV  $l$  or  $i$  so as to avoid such a collision; this is intended to enhance safety awareness, but it could be modified appropriately, if necessary. Therefore, CAV  $i$  will enter the MZ only after  $l$  has exited it, that is,

$$t_i^m \geq t_l^f \quad (14)$$

and  $t_l^f$  is obtained through (5).

(4) Let  $o = \max_j \{j \in \mathcal{O}_i(t)\}$ . In this case, CAV  $o$  is the vehicle immediately ahead of CAV  $i$  in the FIFO queue such that it will not generate any collision with  $i$  in the MZ, so we only require that

$$t_i^f \geq t_o^f \quad (15)$$

and, from (5),  $t_i^m$  is constrained so that

$$t_i^m \geq t_o^f - \Delta_i \quad (16)$$

We are now in a position to establish a lower bound on  $t_i^m$ , the time for CAV  $i$  to enter the MZ, which will serve as a terminal

time constraint in the decentralized optimal control problem considered in Section 4. In so doing, we need to also take into account the lower bound  $t_i^L$  imposed on  $t_i^m$  due to the control and state constraints (2). To derive this lower bound of  $t_i^m$ , we have to consider two cases, which depend on whether CAV  $i$  can reach  $v_{\max}$  upon arriving at the MZ: (i) If CAV  $i$  enters the CZ at  $t_i^0$ , accelerates with  $u_{i,\max}$  until it reaches  $v_{\max}$  and then cruises at this speed until it leaves the MZ at time  $t_i^1$ , it was shown in Zhang

et al. (2016) that  $t_i^1 = t_i^0 + \frac{L}{v_{\max}} + \frac{(v_{\max} - v_i^0)^2}{2u_{i,\max}v_{\max}}$ . (ii) If CAV  $i$  accelerates with  $u_{i,\max}$  but reaches the MZ at  $t_i^m$  with speed  $v_i^m < v_{\max}$ , it was shown in Zhang et al. (2016) that  $t_i^2 = t_i^0 + \frac{\sqrt{2Lu_{i,\max} + (v_i^0)^2} - v_i^0}{u_{\max}}$ . Thus,

$$t_i^L = t_i^1 \mathbb{1}_{v_i^m = v_{\max}} + t_i^2 (1 - \mathbb{1}_{v_i^m = v_{\max}}) \quad (17)$$

The following provides a lower bound for  $t_i^m$  ensuring that is feasible.

**Theorem 1.** The lower bound on the time when CAV  $i$  can enter the MZ and satisfy all MZ safety constraints is given by

$$t_i^m \geq \max\{t_i^L, t_e^f + \frac{\delta}{v_e^f} - \Delta_i, t_s^m + \Delta_s^\delta, t_s^f - \Delta_i, t_l^f, t_o^f - \Delta_i\}, \quad (18)$$

where  $e = \max_j \{j \in \mathcal{E}_i(t)\}$ ,  $s = \max_j \{j \in S_i(t)\}$ ,  $l = \max_j \{j \in \mathcal{L}_i(t)\}$ ,  $o = \max_j \{j \in \mathcal{O}_i(t)\}$  and  $t_i^L$  is given by (17).

**Proof.** If  $\max\{t_i^L, t_e^f + \frac{\delta}{v_e^f} - \Delta_i, t_s^m + \Delta_s^\delta, t_s^f - \Delta_i, t_l^f, t_o^f - \Delta_i\} = t_i^L$ , then  $t_i^m \geq t_i^L$  ensures that  $t_i^m$  is feasible since it depends only on the control and state constraints (2). Let  $j < i$  and  $j \neq e, s, l, o$ . There are four cases to consider as follows.

(1)  $j \in \mathcal{E}_i(t)$ . Since  $e, j \in \mathcal{E}_i(t)$ , CAVs  $e$  and  $j$  are driving towards the same lane. As  $e = \max_r \{r \in \mathcal{E}_i(t)\}$  and  $j \neq e$ , we have  $j < e$  and  $j \in \mathcal{E}_e(t)$ . If  $t_i^m \geq t_e^f + \frac{\delta}{v_e^f} - \Delta_i$ , then (9) holds and we have  $t_i^f \geq t_e^f + \frac{\delta}{v_e^f}$  and  $t_e^f \geq t_j^f + \frac{\delta}{v_j^f}$ , therefore,  $t_i^f > t_j^f + \frac{\delta}{v_j^f}$  which ensures the absence of a rear-end collision at the end of the MZ and (9) holds for all  $j \in \mathcal{E}_i(t)$ .

(2)  $j \in S_i(t)$ . Similarly, since we have  $s, j \in S_i(t)$ , CAVs  $s$  and  $j$  are traveling on the same lane. As  $s = \max_r \{r \in S_i(t)\}$  and  $j \neq s$ , we have  $j < s$  and  $j \in S_s(t)$ . In this case, a rear-end collision at the beginning of the MZ is possible. If  $t_i^m \geq \max\{t_s^m + \Delta_s^\delta, t_s^f - \Delta_i\}$ , then (13) holds and we have  $t_i^f \geq \max\{t_j^m + \Delta_j^\delta + \Delta_s, t_j^f\}$  and  $t_j^f \geq \max\{t_s^m + \Delta_s^\delta + \Delta_i, t_s^f\}$  which leads to  $t_i^f \geq t_j^f$ . Therefore, (6) also holds.

(3)  $j \in \mathcal{L}_i(t)$ . In this case, a lateral collision is possible between  $i$  and  $j$ . Given  $t_i^m \geq t_l^f$ , unlike cases (1) and (2), we cannot determine which subset  $j$  belongs to with respect to CAV  $l$ . To explore the relationship between CAV  $l$  and  $j$  explicitly, there are four subcases to consider as follows. (i)  $j \in \mathcal{E}_i(t)$ . According to (9), we have  $t_i^f > t_j^f$ , therefore,  $t_i^m > t_j^f$  and lateral collision avoidance is ensured. (ii)  $j \in S_i(t)$ . According to (13), we have  $t_i^f \geq \max\{t_j^m + \Delta_j^\delta + \Delta_l, t_j^f\}$  which leads to  $t_i^f \geq t_j^f$ , hence  $t_i^m \geq t_j^f$  and lateral collision avoidance is ensured. (iii)  $j \in \mathcal{L}_i(t)$ . From (14),  $t_i^m \geq t_j^f$  and  $t_i^m \geq t_l^f$ , and it follows that  $t_i^m > t_j^f$  which ensures the absence of a lateral collision. (iv)  $j \in \mathcal{O}_i(t)$ . Based on (15), we have  $t_i^f \geq t_j^f$ . Hence, we still have  $t_i^m \geq t_j^f$  which still ensures lateral collision avoidance.

(4)  $j \in \mathcal{O}_i(t)$ . According to the definition of  $\mathcal{O}_i(t)$ ,  $j$  cannot collide with  $i$ . To summarize, as long as (18) holds, we can guarantee that all MZ constraints are satisfied. ■

Corresponding to the lower bound of terminal time  $t_i^L$ , there also exists the **upper bound**  $t_i^U$ , that is,

$$t_i^U = t_i^3 \mathbb{1}_{v_i^m = v_{\min}} + t_i^4 (1 - \mathbb{1}_{v_i^m = v_{\min}}) \quad (19)$$

where  $v_i(t_i^m) = \sqrt{2Lu_{\min} + (v_i^0)^2}$ , and  $t_i^3 = t_i^0 + \frac{L}{v_{\min}} + \frac{(v_{\min} - v_i^0)^2}{2u_{\min}v_{\min}}$  and  $t_i^4 = t_i^0 + \frac{v_i(t_i^m) - v_i^0}{u_{\min}}$  are derived in a similar way as  $t_i^1$  and  $t_i^2$  in (17) respectively. Based on (19), the following upper bound constraint applies:

$$t_i^m \leq t_i^U \quad (20)$$

It follows directly from (18) that if each CAV seeks to minimize its travel time through the intersection it should select a time  $t_i^m$  given by the lower bound on the right-hand-side. The CAV can then formulate a fixed terminal time optimal control problem with a given objective function and solve this problem in a decentralized way since the value of  $t_i^m$  depends only on information associated with four CAVs (with indices given by  $e, s, l, o < i$ ) whose optimal trajectories have already been determined prior to the arrival of CAV  $i$  at the CZ. This approach was followed in earlier work (Zhang et al., 2016) where no turns were considered. In what follows, we formulate instead a problem that *jointly aims to minimize the travel time of CAV  $i$  along with a measure of its energy consumption*. Therefore, the optimal value of  $t_i^m$  is obtained as part of this problem's solution and the value of Theorem 1, i.e., (18), is to provide a constraint ensuring that this value is feasible.

### 3. Optimal control of CAVs in the CZ

The objective of each CAV inside the CZ, i.e., over  $[t_i^0, t_i^m]$ , is to derive the optimal acceleration/deceleration which minimizes a convex combination of its travel time and energy consumption. For each CAV  $i$ , we define its *information set*  $Y_i(t)$ ,  $t \in [t_i^0, t_i^f]$ , as

$$Y_i(t) \triangleq \{p_i(t), v_i(t), d_i, s_i(t), \mathcal{I}_i\},$$

where  $p_i(t)$ ,  $v_i(t)$  are the traveling distance and speed of CAV  $i$  and  $d_i$  indicates whether  $i$  is making left or right turn or going straight at the MZ. The fourth element in  $Y_i(t)$  is  $s_i(t) = p_k(t) - p_i(t)$ , the inter-vehicle distance between CAV  $i$  and CAV  $k$  which is physically ahead of  $i$  in the same lane (the index  $k$  is made available to  $i$  by the coordinator). Based on this information the *coordinator* can also evaluate

$$\mathcal{I}_i = \{e, s, l, o\}$$

consisting of CAV indices as previously defined for the corresponding sets  $\{\mathcal{E}_i(t), \mathcal{S}_i(t), \mathcal{L}_i(t), \mathcal{O}_i(t)\}$  known to the coordinator. The values of  $e, s, l, o$  are computed when CAV  $i$  arrives at the CZ which is why  $\mathcal{I}_i$  is treated as a time-invariant set. Since the coordinator is not involved in any decision making process regarding vehicle control, we can formulate a tractable decentralized problem, that can be solved on line by each CAV, as follows:

$$\begin{aligned} & \min_{u_i \in U_i} \int_{t_i^0}^{t_i^m} [\gamma_1 + \gamma_2 u_i^2(t)] dt \\ \text{s.t. : } & (1), (2), (3), (18), (20), \\ & p_i(t_i^0) = 0, p_i(t_i^m) = L \\ & \text{and given } t_i^0, v_i(t_i^0), \end{aligned} \quad (21)$$

where  $\gamma_1 = \beta$ ,  $\gamma_2 = \frac{(1-\beta)}{\bar{u}^2}$  with  $\beta \in [0, 1]$  a weight associated with the importance of travel time relative to energy, and  $\bar{u} = \max\{u_{i,\max}, |u_{i,\min}|\}$ . In this manner, we have  $\frac{u_i^2(t)}{\bar{u}^2} \in [0, 1]$  and the overall objective is a well-defined convex combination of the normalized travel time and normalized energy. Note that the objective function in (21) can be rewritten as

$$\gamma_1(t_i^m - t_i^0) + \gamma_2 \int_{t_i^0}^{t_i^m} u_i^2(t) dt$$

**Remark 1.** Unlike the problem considered in Zhang et al. (2016) where  $t_i^m$  was obtained a priori to optimize travel times, here the optimal travel time is determined by the solution of the problem itself. Similarly, the terminal speed  $v_i^m$  is also obtained from the optimal control problem. An alternative formulation is to pre-specify a “target”  $v_i^m$  or to include a penalty term on the deviation of the actual terminal speed from  $v_i^m$ .

#### 3.1. Problem decomposition

In order to simplify notation, we rewrite (21) as

$$\begin{aligned} & \int_{t_i^0}^{t_i^m} \left[ \gamma + \frac{1}{2} u_i^2(t) \right] dt \\ \text{s.t. : } & (1), (2), (3), (18), (20), \\ & p_i(t_i^0) = 0, p_i(t_i^m) = L, \\ & \text{and given } t_i^0, v_i(t_i^0), \end{aligned} \quad (22)$$

where  $\gamma = \frac{\gamma_1}{2\gamma_2}$ . Note that (18) and (20) are constraints applied to the terminal time  $t_i^m$ . In order to efficiently obtain analytical solutions on line, we proceed with a two-step approach. The first step is to consider the following problem by relaxing the terminal time constraints in (22), that is,

$$\begin{aligned} P_0 : & \int_{t_i^0}^{t_i^m} \left[ \gamma + \frac{1}{2} u_i^2(t) \right] dt \\ \text{s.t. : } & (1), (2), (3), \\ & p_i(t_i^0) = 0, p_i(t_i^m) = L, \\ & \text{and given } t_i^0, v_i(t_i^0). \end{aligned} \quad (23)$$

We denote the problem above as  $P_0$ . After solving  $P_0$ , the terminal time obtained is denoted as  $t_i^{m_0}$ . The second step is to check  $t_i^{m_0}$  and (i) If  $t_i^{m_0}$  satisfies both (18) and (20), then  $t_i^{m_0}$  is the optimal terminal time, (ii) If  $t_i^{m_0}$  violates (18), then solve problem  $P_1$  by adding to  $P_0$  the terminal time lower bound constraint from Theorem 1, i.e.,  $t_i^m = \max\{t_i^L, t_e^f + \frac{\delta}{v_e} - \Delta_i, t_s^m + \Delta_s^\delta, t_s^f - \Delta_i, t_l^f, t_o^f - \Delta_i\}$ , (iii) If  $t_i^{m_0}$  violates (20), then solve problem  $P_2$  by adding to  $P_0$  the upper bound terminal time constraint (20)  $t_i^m = t_i^U$ . Note that if  $t_i^L > t_i^U$ , i.e., the lower bound on  $t_i^m$  is higher than its upper bound, the problem is obviously infeasible.

#### 3.2. Analytical solution

Given the objective function of problem  $P_0$ , the Hamiltonian is

$$H_i(p_i, v_i, u_i, \lambda_i, t) = \gamma + \frac{1}{2} u_i^2(t) + \lambda_i^p v_i(t) + \lambda_i^v u_i(t) \quad (24)$$

and the Lagrangian with constraints directly adjoined is

$$\begin{aligned} L_i(p_i, v_i, u_i, \lambda_i, \mu_i, \nu_i, t) = & H_i(p_i, v_i, u_i, \lambda_i, t) + \mu_i g_i(u_i, t) \\ & + \nu_i h_i(p_i, v_i, t) \end{aligned} \quad (25)$$

where (omitting time arguments for simplicity)  $\lambda_i = [\lambda_i^p, \lambda_i^v]^T \in \mathbb{R}^2$  is the costate vector,  $g_i(u_i, t) \leq 0$  and  $h_i(p_i, v_i, t) \leq 0$  represents the control constraints and state constraints respectively, and  $\mu_i = [\mu_i^a, \mu_i^b]^T \in \mathbb{R}^2$ ,  $\nu_i = [\nu_i^e, \nu_i^d, \nu_i^s]^T \in \mathbb{R}^3$  are *Lagrange multipliers* with

$$\mu_i^a = \begin{cases} > 0, & u_i(t) - u_{\max} = 0, \\ = 0, & u_i(t) - u_{\max} < 0, \end{cases} \quad (26)$$

$$\mu_i^b = \begin{cases} > 0, & u_{\min} - u_i(t) = 0, \\ = 0, & u_{\min} - u_i(t) < 0, \end{cases} \quad (27)$$

$$\nu_i^e = \begin{cases} > 0, & v_i(t) - v_{\max} = 0, \\ = 0, & v_i(t) - v_{\max} < 0, \end{cases} \quad (28)$$

$$v_i^d = \begin{cases} > 0, & v_{\min} - v_i(t) = 0, \\ = 0, & v_{\min} - v_i(t) < 0. \end{cases} \quad (29)$$

$$v_i^s = \begin{cases} > 0, & p_i(t) + \delta - p_k(t) = 0, \\ = 0, & p_i(t) + \delta - p_k(t) < 0. \end{cases} \quad (30)$$

where  $k$  is the CAV physically ahead of  $i$  in the same lane and its position  $p_k(t)$  is known to  $i$  through the coordinator (or through on-board sensors).

The Euler–Lagrange equations become

$$\dot{\lambda}_i^p(t) = -\frac{\partial L_i}{\partial p_i} = \begin{cases} 0, & p_i(t) + \delta - p_k(t) < 0, \\ -v_i^s, & p_i(t) + \delta - p_k(t) = 0, \end{cases} \quad (31)$$

and

$$\dot{\lambda}_i^v(t) = -\frac{\partial L_i}{\partial v_i} = \begin{cases} -\lambda_i^p(t), & v_i(t) - v_{\max} < 0 \text{ and} \\ & v_{\min} - v_i(t) < 0, \\ -\lambda_i^p(t) - v_i^c, & v_i(t) - v_{\max} = 0, \\ -\lambda_i^p(t) + v_i^d, & v_{\min} - v_i(t) = 0. \end{cases} \quad (32)$$

Since the terminal time  $t_i^m$  and terminal speed  $v_i^m$  are not fixed, we have the transversality conditions

$$\lambda_i^v(t_i^m) = 0, \quad H_i(t_i^m) = 0 \quad (33)$$

Note that if we need to solve  $P_1$  and  $P_2$ , then the second equation in (41) no longer holds; instead,  $t_i^m$  is fixed to its upper or lower bound as described above. In addition, there also exist the state boundary conditions  $p_i(t_i^0) = 0$ ,  $p_i(t_i^m) = L$ ,  $v_i(t_i^0) = v_i^0$ , given the initial time  $t_i^0$  and the initial speed  $v_i^0$ .

The necessary condition for optimality is

$$\frac{\partial L_i}{\partial u_i} = \begin{cases} u_i(t) + \lambda_i^v(t), & u_i(t) - u_{\max} < 0 \text{ and} \\ & u_{\min} - u_i(t) < 0, \\ u_i(t) + \lambda_i^v(t) + \mu_i^a, & u_i(t) - u_{\max} = 0, \\ u_i(t) + \lambda_i^v(t) - \mu_i^b, & u_{\min} - u_i(t) = 0. \end{cases} \quad (34)$$

A complete solution of this problem requires that constrained and unconstrained arcs of an optimal trajectory are pieced together to satisfy all conditions (26) through (34). This includes the five constraints (three pure-state constraints, two control constraints) in (26) through (30). While there are many different cases that can occur, the nature of the optimal solution rules out the possibility of several cases. In what follows, we provide a complete analysis of the case where no constraints are active and of the case where the safety constraint  $p_i(t) + \delta - p_k(t) \leq 0$  is the only active one. A discussion of the remaining cases can be found in Appendix A.

### 3.3. Unconstrained optimal control analysis

For problem  $P_0$ , the terminal time is free whereas for  $P_1$  and  $P_2$  the terminal time is fixed. Thus, we provide the analysis for each of these two cases.

#### 3.3.1. Free terminal time

When the state and control constraints are inactive, we have  $\mu_i^a = \mu_i^b = v_i^c = v_i^d = v_i^s = 0$ . The Lagrangian (25) becomes  $L_i(p, v, u, \lambda, \mu, v, t) = H_i(p, v, u, \lambda, t)$  and (34) reduces to  $\frac{\partial L_i}{\partial u_i} = u_i(t) + \lambda_i^v = 0$ , which leads to

$$u_i(t) = -\lambda_i^v(t). \quad (35)$$

Since  $v_i^s = 0$ , (31) becomes  $\dot{\lambda}_i^p(t) = -\frac{\partial L_i}{\partial p_i} = 0$  which leads to

$$\lambda_i^p = a_i \quad (36)$$

where  $a_i$  is a constant. Since  $v_i^c = v_i^d = 0$ , (32) becomes  $\dot{\lambda}_i^v(t) = -\frac{\partial L_i}{\partial v_i} = -\lambda_i^p$ . Since  $\lambda_i^p = a_i$ , we have

$$\lambda_i^v(t) = -a_i t - b_i \quad (37)$$

where  $b_i$  is a constant. We can now obtain a complete analytical solution of  $P_0$  as follows.

**Theorem 2.** The optimal trajectory for problem  $P_0$  is given by

$$u_i^*(t) = a_i t + b_i \quad (38)$$

$$v_i^*(t) = \frac{1}{2} a_i t^2 + b_i t + c_i \quad (39)$$

$$p_i^*(t) = \frac{1}{6} a_i t^3 + \frac{1}{2} b_i t^2 + c_i t + d_i \quad (40)$$

for  $t \in [t_i^0, t_i^{m*}]$  where  $a_i$ ,  $b_i$ ,  $c_i$  and  $d_i$  are constants determined along with  $t_i^{m*}$  through

$$\frac{1}{6} a_i \cdot (t_i^0)^3 + \frac{1}{2} b_i \cdot (t_i^0)^2 + c_i t_i^0 + d_i = 0 \quad (41a)$$

$$\frac{1}{2} a_i \cdot (t_i^0)^2 + b_i t_i^0 + c_i = v_i^0 \quad (41b)$$

$$\frac{1}{6} a_i \cdot (t_i^m)^3 + \frac{1}{2} b_i \cdot (t_i^m)^2 + c_i t_i^m + d_i = L \quad (41c)$$

$$a_i t_i^m + b_i = 0 \quad (41d)$$

$$\gamma - \frac{1}{2} b_i^2 + a_i c_i = 0 \quad (41e)$$

**Proof.** The optimal control in (38) follows from (35) and (37). Using (38) in the system dynamics (1), we then derive (39) and (40). Next, (41a) through (41c) follow from the boundary conditions  $p_i(t_i^0) = 0$ ,  $v_i(t_i^0) = v_i^0$ ,  $p_i(t_i^m) = L$  and (41d) follows from  $\lambda_i^v(t_i^m) = 0$  in (33) and from (38). The last equation follows from  $H_i(t_i^m) = 0$  in (33):

$$\begin{aligned} \gamma + \frac{1}{2} (u_i^*(t_i^m))^2 + a_i v_i^*(t_i^m) - (u_i^*(t_i^m))^2 \\ = \gamma - \frac{1}{2} (a_i t_i^m + b_i)^2 + a_i \left( \frac{1}{2} a_i (t_i^m)^2 + b_i t_i^m + c_i \right) \\ = \gamma - \frac{1}{2} b_i^2 + a_i c_i = 0 \end{aligned}$$

using (24), (36), (37), (38) and (39). ■

Thus, a complete solution of  $P_0$  boils down to solving the five equations in (41). A typical simulation example of this case can be found in Section 5.

The next two results establish a basic property of the optimal control, i.e., it is non-negative and non-increasing, and the fact that two of the constraints in (2) cannot be active.

**Lemma 1.** For the unconstrained problem with free terminal time, the optimal control is non-negative, i.e.,  $u_i^*(t) \geq 0$ , and monotonically non-increasing

**Proof.** See Appendix B.

**Lemma 2.** For the unconstrained problem with free terminal time, it is not possible for constraints  $v_{\min} - v_i(t) \leq 0$  and/or  $u_{\min} - u_i(t) \leq 0$  to become active.

**Proof.** See Appendix B.

#### 3.3.2. Fixed terminal time

If the terminal time  $t_i^{m*}$  obtained from solving  $P_0$  turns out to violate (18) or (20), then, as described in the two-step approach earlier, we need to solve either  $P_1$  or  $P_2$  by setting  $t_i^m$  to a fixed value which is either the lower bound in (18) or the upper bound in (20). Therefore, the transversality condition  $H_i(t_i^m) = 0$ , i.e., the

fifth equation in (41a), no longer holds and the solution of this problem reduces to

$$\begin{bmatrix} \frac{1}{6}(t_i^0)^3 & \frac{1}{2}(t_i^0)^2 & t_i^0 & 1 \\ \frac{1}{2}(t_i^0)^2 & t_i^0 & 1 & 0 \\ \frac{1}{6}(t_i^m)^3 & \frac{1}{2}(t_i^m)^2 & t_i^m & 1 \\ t_i^m & 1 & 0 & 0 \end{bmatrix} \cdot \begin{bmatrix} a_i \\ b_i \\ c_i \\ d_i \end{bmatrix} = \begin{bmatrix} 0 \\ v_i^0 \\ L \\ 0 \end{bmatrix} \quad (42)$$

which yields the four parameters  $a_i, b_i, c_i, d_i$  from a simple system of linear equations. A typical simulation example of this case when (18) is violated can be found in Section 5.

With the terminal time fixed, Lemma 1 needs to be modified as follows.

**Lemma 3.** *For the unconstrained problem with fixed terminal time, the optimal control must be either monotonically non-increasing and  $u_i^*(t) \geq 0$ , or monotonically non-decreasing and  $u_i^*(t) \leq 0$ .*

**Proof.** See Appendix B.

### 3.4. Constrained optimal control analysis

Checking whether the optimal solution of the unconstrained problem  $P_0, P_1$  or  $P_2$  violates any of the constraints (26) through (30) is easily accomplished since the unconstrained optimal control in (38) is a linear function of time and the optimal speed is a quadratic function of time. When this happens, we must check whether there exists a nonempty feasible control set. One approach followed in earlier work (Zhang et al., 2017) is to identify the set of all initial conditions  $(t_i^0, v_i^0)$  such that no constraint is violated over  $[t_i^0, t_i^m]$  or at least some of the constraints are not violated while the rest are explicitly dealt with through the Lagrangian in (25). As shown in Zhang et al. (2017), it is possible to define a Feasibility Enforcement Zone (FEZ) which precedes the CZ such that each CAV is controlled over the FEZ so as to reach a feasible initial condition when reaching the CZ. Here, however, we proceed differently by following a direct approach through which we derive explicit solutions for any feasible optimal constrained trajectory. In so doing, we can also explicitly identify when an optimal solution is infeasible under initial conditions  $(t_i^0, v_i^0)$ .

When the optimal solution of the unconstrained problem violates a constraint, we need to re-solve the problem by identifying an optimal trajectory that includes unconstrained arcs pieced together with one or more constrained arcs such that all necessary conditions for optimality are satisfied. For a control constraint of the form  $g_i(u_i, t) \leq 0$  as in (26)–(27), the optimal control on a constrained arc can be simply obtained by solving  $g_i(u_i, t) = 0$ . The remaining constraints (28)–(30) in our problem are pure state constraints of the form  $h_i(x_i, t) \leq 0$ . In this case (see Bryson & Ho, 1975), we define the tangency constraints

$$N_i(x_i, t) \triangleq [h_i(x_i, t) \ h_i^{(1)}(x_i, t) \ \cdots \ h_i^{(q-1)}(x_i, t)]^T = 0, \quad (43)$$

where  $h_i^{(k)}(x_i, t)$  is the  $k$ th time derivative and  $q$  derivatives are taken until we obtain an expression that explicitly depends on the control  $u_i$  so that

$$h_i^{(q)}(x_i, t) = 0. \quad (44)$$

At the junction points of constrained and unconstrained arcs, the costate and Hamiltonian trajectories may have discontinuities. This can be determined using the following jump conditions (Bryson & Ho, 1975), where  $\tau$  denotes a junction point and

$\tau^-, \tau^+$  denote the left-hand side and the right-hand side limits, respectively:

$$\begin{aligned} \lambda_i(\tau^-) &= \lambda_i(\tau^+) + \pi_i^T \frac{\partial N_i(x_i, t)}{\partial x_i}, \\ H_i(\tau^-) &= H_i(\tau^+) - \pi_i^T \frac{\partial N_i(x_i, t)}{\partial t}. \end{aligned} \quad (45)$$

where  $N_i(x_i, t)$  is the  $q$ -dimensional vector in (43) and  $\pi_i$  is a  $q$ -dimensional vector of constant Lagrange multipliers satisfying  $\pi_i^T N_i(x_i, t) = 0$  and  $\pi_i \geq 0, i = 1, \dots, q$ . Consequently, the optimal control  $u_i^*(t)$  may or may not be continuous at junction points.

In what follows, we concentrate on the safety constraint (3) which is the most challenging to deal with. In this case, we have  $\mu_i^a = \mu_i^b = v_i^c = v_i^d = 0$ . The remaining constraints are discussed in the Appendix. Thus, we set  $h_i(p_i, t) = p_i + \delta - p_k^*(t)$  where we observe that  $p_k^*(t)$  is a known explicit function of time given by the optimal position trajectory of CAV  $k$  specified in (41) or (42) since, upon arrival of CAV  $i$  at the CZ, the optimal solution of the problem associated with  $k < i$  has already been fully determined. Moreover,  $h_i^{(1)}(p_i, t) = v_i - \frac{\partial p_k^*(t)}{\partial t} = v_i - v_k^*(t)$  where  $v_k^*(t)$  is also an explicit function of time in (41) or (42) and  $h_i^{(2)}(p_i, t) = u_i - \frac{\partial v_k^*(t)}{\partial t} = u_i - u_k^*(t)$ , hence the optimal control on the constrained arc is given by  $u_i^*(t) = u_k^*(t)$ .

The following result establishes the continuity property of the optimal control when the trajectory enters a constrained arc where  $p_i(t) + \delta - p_k^*(t) = 0$ .

**Theorem 3.** *The optimal control  $u_i^*(t)$  is continuous at the junction  $\tau$  of the unconstrained and safety-constrained arcs, i.e.,  $u_i^*(\tau^-) = u_i^*(\tau^+)$ .*

**Proof.** By assumption, the rear-end safety constraint is not active at  $t_i^0$ . Hence, when the safety constraint  $p_i(t) + \delta - p_k^*(t) \leq 0$  becomes active,  $\tau$  is the entry time of the constrained arc, and the jump conditions in (45) become

$$\begin{aligned} \lambda_i^p(\tau^-) &= \lambda_i^p(\tau^+) + \pi_i^p \frac{\partial}{\partial p_i} [p_i + \delta - p_k^*(t)] \\ \lambda_i^v(\tau^-) &= \lambda_i^v(\tau^+) + \pi_i^v \frac{\partial}{\partial v_i} [v_i - v_k^*(t)] \\ H_i(\tau^-) &= H_i(\tau^+) - \pi_i^p \frac{\partial}{\partial t} [p_i + \delta - p_k^*(t)] - \pi_i^v \frac{\partial}{\partial t} [v_i - v_k^*(t)] \end{aligned}$$

where  $\frac{\partial p_k^*(t)}{\partial t} = v_k^*(t)$  and  $\frac{\partial v_k^*(t)}{\partial t} = u_k^*(t)$  are explicit functions of  $t$  specified through (41) or (42). We assume that  $u_k^*(t)$ ,  $k < i$ , is continuous in  $t$  so that, if we can establish that  $u_k^*(t)$  is continuous, then a simple iterative argument completes the proof. The equations above become

$$\begin{aligned} \lambda_i^p(\tau^-) &= \lambda_i^p(\tau^+) + \pi_i^p, \quad \lambda_i^v(\tau^-) = \lambda_i^v(\tau^+) + \pi_i^v, \\ H_i(\tau^-) &= H_i(\tau^+) + \pi_i^p v_k^*(t) + \pi_i^v u_k^*(t) \end{aligned}$$

For  $t \geq \tau^+$ , the tangency conditions (43)–(44) with  $q = 2$  hold:

$$\begin{aligned} p_i(t) + \delta - p_k^*(t) &= 0 \\ v_i(t) - v_k^*(t) &= 0 \\ u_i(t) - u_k^*(t) &= 0 \end{aligned}$$

In addition, note that the position  $p_i(t)$  and speed  $v_i(t)$  are continuous functions of  $t$ . Combining the equations above and recalling from (24) that  $H_i(t) = \gamma + \frac{1}{2}u_i^2(t) + \lambda_i^p(t)v_i(t) + \lambda_i^v(t)u_i(t)$ , we get

$$\begin{aligned} &\gamma + \frac{1}{2}u_i^2(\tau^-) + \lambda_i^p(\tau^-)v_i(\tau) + \lambda_i^v(\tau^-)u_i(\tau^-) \\ &= \gamma + \frac{1}{2}u_i^2(\tau^+) + \lambda_i^p(\tau^+)v_i(\tau) + \lambda_i^v(\tau^+)u_i(\tau^+) \\ &\quad + \pi_i^p v_k^*(\tau) + \pi_i^v u_k^*(\tau) \end{aligned}$$



and since  $u_i(\tau^+) = u_k^*(\tau)$ , it follows that

$$\begin{aligned} & \frac{1}{2}u_i^2(\tau^-) - \frac{1}{2}u_i^2(\tau^+) + [\lambda_i^p(\tau^-) - \lambda_i^p(\tau^+)]v_k^*(\tau) \\ & - \pi_i^p v_k^*(\tau) + \lambda_i^v(\tau^-)u_i(\tau^-) - \lambda_i^v(\tau^+)u_i(\tau^+) - \pi_i^v u_i(\tau^+) = 0 \end{aligned}$$

which reduces to

$$\begin{aligned} & \frac{1}{2}u_i^2(\tau^-) - \frac{1}{2}u_i^2(\tau^+) + \lambda_i^v(\tau^-)[u_i(\tau^-) - u_i(\tau^+)] \\ & = [u_i(\tau^-) - u_i(\tau^+)](\frac{1}{2}[u_i(\tau^-) + u_i(\tau^+)] + \lambda_i^v(\tau^-)) = 0 \end{aligned}$$

Therefore, either  $u_i(\tau^-) - u_i(\tau^+) = 0$ , or  $\frac{1}{2}[u_i(\tau^-) + u_i(\tau^+)] + \lambda_i^v(\tau^-) = 0$ . Assuming that  $u_i(\tau^-) - u_i(\tau^+) \neq 0$ , recall that at  $\tau^-$  the trajectory arc is unconstrained so that (35) holds:  $u_i(\tau^-) = -\lambda_i^v(\tau^-)$  and it follows that  $u_i(\tau^-) - u_i(\tau^+) = 0$ . We conclude that  $u_i(t)$  is continuous at  $\tau$  and the proof is complete. ■

Once an optimal trajectory for CAV  $i$  enters the constrained arc  $p_i(t) + \delta - p_k^*(t) = 0$ , it may remain on this arc through the terminal time  $t_i^m$  or exit it at some point  $\tau' > \tau$  and follow an unconstrained arc over  $[\tau', t_i^m]$ . This depends on whether such an exit point  $\tau'$  is feasible on an optimal trajectory. More generally, it is possible that an optimal trajectory consists of a sequence of alternating unconstrained and constrained arcs whose feasibility needs to be checked. Thus, once we establish that an optimal trajectory contains a constrained arc, there are two cases to consider.

**Case 1:** No exit point from the constrained arc. In this case, CAV  $i$  remains on the constrained arc until it reaches the MZ and we have

$$u_i^*(t) = \begin{cases} a_i t + b_i & t \in [t_i^0, \tau] \\ u_k^*(t) & t \in (\tau, t_i^m] \end{cases} \quad (46)$$

Moreover,  $v_i^*(t)$  is given by (39) for  $t \in [t_i^0, \tau]$  and  $v_i^*(t) = v_k^*(t)$  for  $t \in (\tau, t_i^m]$ ;  $p_i^*(t)$  is given by (40) for  $t \in [t_i^0, \tau]$  and  $p_i^*(t) + \delta - p_k^*(t) = 0$  for  $t \in (\tau, t_i^m]$ . The constants  $a_i, b_i, c_i$  and  $d_i$  along with  $\tau$  are determined through

$$\frac{1}{6}a_i \cdot (t_i^0)^3 + \frac{1}{2}b_i \cdot (t_i^0)^2 + c_i t_i^0 + d_i = 0 \quad (47a)$$

$$\frac{1}{2}a_i \cdot (t_i^0)^2 + b_i t_i^0 + c_i = v_i^0 \quad (47b)$$

$$a_i \tau + b_i = u_k^*(\tau) \quad (47c)$$

$$\frac{1}{6}a_i \tau^3 + \frac{1}{2}b_i \tau^2 + c_i \tau + d_i + \delta = p_k^*(\tau) \quad (47d)$$

$$\frac{1}{2}a_i \tau^2 + b_i \tau + c_i = v_k^*(\tau) \quad (47e)$$

The first two equations above are the same as in (41) and follow from the initial conditions, while (47c) follows from (46) and Theorem 3. In addition, (47d) follows from (47a) when the safety constraint becomes active, i.e.,  $p_i^*(\tau) + \delta - p_k^*(\tau) = 0$ , and (47e) follows from  $v_i^*(\tau) = v_k^*(\tau)$ . Note that in this case the terminal time  $t_i^m$  is fixed and determined by CAV  $s$  in (18). A typical simulation example of this case is given in Section 5 (Fig. 5).

**Remark 2.** As noted in Section 2, an alternative to the distance-based safety constraint  $p_k(t) - p_i(t) \geq \delta$  is the speed-based safety constraint (Rajamani et al., 2000)  $p_k(t) - p_i(t) \geq \varphi v_i(t) + \delta$ . While the expression of the analytical solutions becomes more complicated, the approach for deriving all necessary conditions is the same as described above.

**Case 2:** There exists an exit point from the constrained arc. In this case, letting  $\tau_1$  denote the entry point to the constrained arc and  $\tau_2$  the exit point, there are two subcases to consider: (i) when the terminal time  $t_i^m$  is free, and (ii) when the terminal time is

fixed. When the terminal time is free, the transversality condition (33) holds, and a solution is obtained through the system of five equations in (47) with  $\tau_1$  replacing  $\tau$  along with the following equations:

$$e_i \tau_2 + r_i = u_k^*(\tau_2) \quad (48a)$$

$$\frac{1}{6}e_i \tau_2^3 + \frac{1}{2}r_i \tau_2^2 + q_i \tau_2 + m_i + \delta = p_k^*(\tau_2) \quad (48b)$$

$$\frac{1}{2}e_i \tau_2^2 + r_i \tau_2 + q_i = v_k^*(\tau_2) \quad (48c)$$

$$\frac{1}{6}e_i \cdot (t_i^m)^3 + \frac{1}{2}r_i \cdot (t_i^m)^2 + q_i t_i^m + m_i = L \quad (48d)$$

$$e_i t_i^m + r_i = 0 \quad (48e)$$

$$\gamma - \frac{1}{2}r_i^2 + e_i q_i = 0. \quad (48f)$$

The first equation above follows from the fact that  $[\tau_2, t_i^m]$  is an unconstrained arc so that (38) applies but with new constants  $e_i, r_i$  and from  $u_i^*(\tau_2^-) = u_i^*(\tau_2^+) = u_k^*(\tau_2)$ ; (48b) follows from the constraint  $p_i^*(\tau_2) + \delta - p_k^*(\tau_2) = 0$  and (48c) from  $v_i^*(\tau_2) = v_k^*(\tau_2)$ . Next, (48d) is the boundary constraint  $p_i^*(t_i^m) = L$ , while (48e) and (48f) are the transversality conditions similar to the last two equations in (41). A simulation example of this case is given in Section 5 (Fig. 6). In the case where the terminal time  $t_i^m$  is fixed (as in problems  $P_1$  and  $P_2$ ) we simply remove the transversality condition in the last equation above.

**Remark 3.** Note that  $a_i, b_i, c_i, d_i$  and  $\tau_1$  can be determined from the five equations in (47) independently from  $e_i, r_i, q_i, m_i$  and  $\tau_2$  in (48). Thus, the construction of an optimal trajectory is obtained by solving two sub-problems and piecing the solutions together. This is an important property because it also allows us to easily check for the existence of a feasible solution: if  $\tau_2 < \tau_1$  then no feasible optimal trajectory exists in this case.

#### 4. Optimal control of CAVs in the MZ

As mentioned in Section 2.1, the inclusion of left and right turns requires consideration of passenger comfort which is commonly quantified through the jerk  $J_i(t) = \dot{u}_i(t)$  (Hogan, 1984) defined as the time derivative of acceleration. Thus, one approach to minimize passenger discomfort in the MZ is to keep the magnitude of the resultant force, which consists of the centripetal force and the braking force, unchanged. Note that both the magnitude of the centripetal force and the angle between the centripetal and braking forces do not change while the vehicle makes a turn. Hence, the following optimization problem is formulated with the objective of minimizing the  $L^2$ -norm of jerk for each CAV  $i$ :

$$\begin{aligned} & \min_{J_i} \frac{1}{2} \int_{t_i^m}^{t_i^f} J_i^2(t) dt \\ & \text{s.t. : } (1), J_i(t) = \dot{u}_i(t), \end{aligned} \quad (49)$$

$$\begin{aligned} & \text{given } t_i^m, t_i^f, u_i(t_i^m), u_i(t_i^f), \\ & v_i^m, v_i^f, p_i(t_i^m), p_i(t_i^f). \end{aligned}$$

and, following the definitions in Section 2.1, we have

$$\begin{aligned} & p_i(t_i^m) = L, \\ & p_i(t_i^f) = \begin{cases} L + S_L, & \text{if } d_i = 0, \\ L + S, & \text{if } d_i = 1, \\ L + S_R, & \text{if } d_i = 2, \end{cases} \end{aligned} \quad (50)$$

The analytical solution of problem (49) was obtained in Ntousakis, Nikolos, and Papageorgiou (2016) using Hamiltonian analysis and considering the jerk as the control input.

#### 4.1. Joint minimization of passenger discomfort and energy consumption

In dealing with turning CAVs in the MZ, we formulate a joint objective expressed as a convex combination of acceleration/deceleration and jerk as follows:

$$\min_{J_i} \frac{1}{2} \int_{t_i^m}^{t_i^f} [\rho_1 u_i^2(t) + \rho_2 J_i^2(t)] dt \quad (51)$$

$$\text{s.t. : (1), } J_i(t) = \dot{u}_i(t),$$

given  $t_i^m, t_i^f, u_i(t_i^m), v_i^m, (50), v_i^f$ .

where  $\rho_1 = w \cdot q_1, \rho_2 = (1 - w) \cdot q_2$  with  $q_1, q_2$  being the normalization factors which are selected so that  $q_1 \cdot u_i^2 \in [0, 1]$  and  $q_2 \cdot J_i^2 \in [0, 1]$ , and  $w \in [0, 1]$  is a weight associated with the importance of energy consumption relative to passenger discomfort. Note that  $t_i^m$  has already been determined by solving the CZ optimal control problem in the previous section, hence also  $u_i(t_i^m)$  and  $v_i^m$  are known. Finally,  $v_i^f$  is also set to a constant  $v_i^f = v^f$  for all CAVs, where  $v^f$  is a predetermined desired exit speed (e.g.,  $v_{\max}$  if we wish to maximize traffic throughput after the intersection). The reason for selecting a common speed is to prevent the chance of collisions that might result when CAVs exit the MZ at different speeds.

Given the objective function in (51), the Hamiltonian is

$$H_i(p_i, v_i, u_i, J_i, \lambda_i, t) = \frac{1}{2} [\rho_1 u_i^2(t) + \rho_2 J_i^2(t)] + \lambda_i^p v_i(t) + \lambda_i^v u_i(t) + \lambda_i^u J_i(t), \quad (52)$$

where  $\lambda_i^p, \lambda_i^v, \lambda_i^u$  are the costate variables. Note that the collision avoidance inside the MZ has been ensured through (18). The Euler–Lagrange equations associated with the position and speed respectively are

$$\dot{\lambda}_i^p = -\frac{\partial H_i}{\partial p_i} = 0, \quad \dot{\lambda}_i^v = -\frac{\partial H_i}{\partial v_i} = -\lambda_i^p, \quad (53)$$

and

$$\dot{\lambda}_i^u = -\frac{\partial H_i}{\partial u_i} = -\rho_1 u_i - \lambda_i^v, \quad (54)$$

is associated with the acceleration. Since the terminal acceleration/deceleration  $u_i(t_i^f)$  is not pre-specified, we also have the transversality condition

$$\lambda_i^u(t_i^f) = 0. \quad (55)$$

The necessary condition for optimality is

$$\frac{\partial H_i}{\partial J_i} = \rho_2 J_i(t) + \lambda_i^u = 0, \quad (56)$$

Note that (53) leads to

$$\lambda_i^p = a_i, \text{ and } \lambda_i^v = -a_i t - b_i, \quad (57)$$

where  $a_i$  and  $b_i$  are constants of integration. Given (54), we have

$$\lambda_i^u = \frac{1}{2} a_i t^2 + b_i t - \rho_1 v_i + c_i \quad (58)$$

where  $c_i$  is a constant. We can now obtain a complete analytical solution of (51) as follows.

**Theorem 4.** The optimal trajectory for (51) is given by

$$J_i^*(t) = \frac{a_i}{\rho_1} + e_i A_1^3 e^{A_1 t} + f_i A_2^3 e^{A_2 t} \quad (59)$$

$$u_i^*(t) = \frac{1}{\rho_1} (a_i t + b_i) + e_i A_1^2 e^{A_1 t} + f_i A_2^2 e^{A_2 t} \quad (60)$$

$$v_i^*(t) = \frac{1}{\rho_1} \left( \frac{1}{2} a_i t^2 + b_i t + c_i + \frac{a_i \rho_2}{\rho_1} \right) + d_i A_1 e^{A_1 t} + f_i A_2 e^{A_2 t} \quad (61)$$

$$p_i^*(t) = \frac{1}{\rho_1} \left( \frac{1}{6} a_i t^3 + \frac{1}{2} b_i t^2 + c_i t + \frac{a_i \rho_2}{\rho_1} t + d_i \right) + e_i e^{A_1 t} + f_i e^{A_2 t} \quad (62)$$

where  $A_1 = \sqrt{\frac{\rho_1}{\rho_2}}, A_2 = -\sqrt{\frac{\rho_1}{\rho_2}}$ , and  $a_i, b_i, c_i, d_i, e_i$  and  $f_i$  are constants of integration determined through

$$\frac{1}{\rho_1} \left( \frac{1}{6} a_i \cdot (t_i^m)^3 + \frac{1}{2} b_i \cdot (t_i^m)^2 + c_i t_i^m + \frac{a_i \rho_2}{\rho_1} t_i^m + d_i \right) + e_i e^{A_1 t_i^m} + f_i e^{A_2 t_i^m} = L \quad (63a)$$

$$\frac{1}{\rho_1} \left( \frac{1}{2} a_i \cdot (t_i^m)^2 + b_i t_i^m + c_i + \frac{a_i \rho_2}{\rho_1} \right) + d_i A_1 e^{A_1 t_i^m} + f_i A_2 e^{A_2 t_i^m} = v_i^m \quad (63b)$$

$$\frac{1}{\rho_1} (a_i t_i^m + b_i) + e_i A_1^2 e^{A_1 t_i^m} + f_i A_2^2 e^{A_2 t_i^m} = u_i^m \quad (63c)$$

$$\frac{1}{\rho_1} \left( \frac{1}{6} a_i \cdot (t_i^f)^3 + \frac{1}{2} b_i \cdot (t_i^f)^2 + c_i t_i^f + \frac{a_i \rho_2}{\rho_1} t_i^f + d_i \right) + e_i e^{A_1 t_i^f} + f_i e^{A_2 t_i^f} = p_i^f \quad (63d)$$

$$\frac{1}{\rho_1} \left( \frac{1}{2} a_i \cdot (t_i^f)^2 + b_i t_i^f + c_i + \frac{a_i \rho_2}{\rho_1} \right) + d_i A_1 e^{A_1 t_i^f} + f_i A_2 e^{A_2 t_i^f} = v_i^f \quad (63e)$$

$$\frac{a_i}{\rho_1} + e_i A_1^3 e^{A_1 t_i^f} + f_i A_2^3 e^{A_2 t_i^f} = 0. \quad (63f)$$

**Proof.** Combining (58) with (56), we have the ordinary differential equation:

$$\rho_2 \ddot{v}_i - \rho_1 v_i + \frac{1}{2} a_i t^2 + b_i t + c_i = 0.$$

whose solution yields the optimal speed (61). Using (61) in the system dynamics, we can then derive (59), (60) and (62). The first five equations in (63) follow from the boundary conditions  $p_i(t_i^m) = L, v_i(t_i^m)$  and  $u_i(t_i^m)$  (known by  $t_i^m$ ), and the specified  $p_i(t_i^f)$  and  $v_i(t_i^f)$ . The last equation follows from the transversality condition (55):

$$\begin{aligned} \lambda_i^u(t_i^f) &= -\frac{J_i(t_i^f)}{\rho_2} \\ &= \rho_2 \left[ \frac{a_i}{\rho_1} + e_i A_1^3 e^{A_1 t_i^f} + f_i A_2^3 e^{A_2 t_i^f} \right] = 0. \end{aligned}$$

using (59). ■

Note that since  $0 \leq w \leq 1$ , the optimal solution is only valid when  $w \neq 1$  and  $w \neq 0$ . When  $w = 0$ , the problem becomes (49) with the objective of minimizing jerk only. When  $w = 1$ , the problem minimizes energy consumption only. Although the state and control constraints are not incorporated in (51), it is possible that the minimum speed  $v_{\min}$  and/or maximum deceleration  $u_{\min}$  constraints become active. The approach to analyze such cases is similar to the analysis in Appendix A.

## 5. Simulation examples

We begin with several numerical examples illustrating the different cases discussed in Section 3. In terms of computational complexity, we should point out that except for the case where the complete solution is given by the simple system of linear

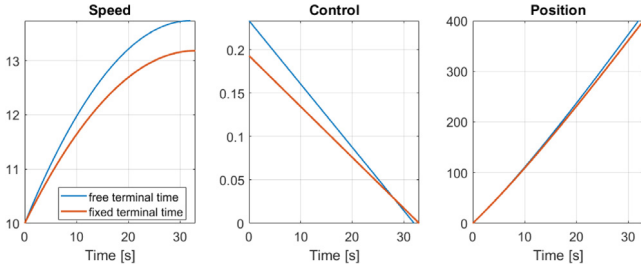


**Fig. 4.** Unconstrained optimal trajectories with free and fixed terminal times. (For interpretation of the references to color in this figure legend, the reader is referred to the web version of this article.)

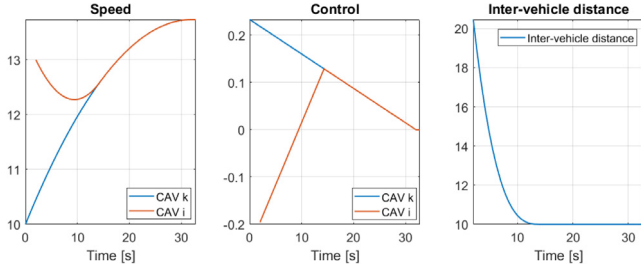


**Fig. 5.** The state constraint  $p_i(t) + \delta - p_k(t) \leq 0$  active (no exit).

equations (42), solving a system of nonlinear equations with six parameters involved as in (48) is certainly nontrivial. A good initial ‘guess’ of the parameter values is extremely useful in the convergence of the root-finding algorithm for numerical solvers. To do so, our approach is to start with the unconstrained optimal solution and add the constraints step by step. At each step, when a constraint is added to the problem, we use the solution from the previous step as the initial estimate and obtain the new solution, which is then used as the initial estimate for the problem formulated in the next step; if the current solution satisfies all the constraints, then we have obtained the optimal solution.

*Unconstrained optimal control with free terminal time.* The parameters used are:  $L = 400$  m,  $\gamma = 0.1$ ,  $v_i^0 = 10$  m/s,  $t_i^0 = 0$  s. The optimal terminal time is obtained as  $t_i^m = 32.03$  s as shown by the blue curves in Fig. 4.

*Unconstrained optimal control with fixed terminal time.* Assuming  $t_i^m = 32.03$  s violates (18), and we need to formulate problem  $P_1$  by adding  $t_i^m = 33$  s to  $P_0$ . The resulting optimal control, speed, and position trajectories are shown by the red curves in Fig. 4.

*Safety-constrained optimal control without exit.* Assuming CAV  $k = 1$  enters the CZ at  $t_k^0 = 0$  with an initial speed  $v_k^0 = 10$  m/s and exits at  $t_k^m = 32.03$  s, the optimal control is  $u_k^*(t) = -0.0073t + 0.23$ . Then, we assume that CAV  $i = 2$  enters the CZ at  $t_i^0 = 2$  s with an initial speed  $v_i^0 = 13$  m/s. The terminal time of CAV  $i$  is  $t_i^m = t_k^m + \frac{\delta}{v_k^m} = 32.76$  s where the minimal safe following distance is  $\delta = 10$  m. The optimal control for CAV  $i$  is

$$u_i^*(t) = \begin{cases} 0.0263t - 0.25, & t \in [2, 14.31] \\ -0.0073t + 0.23, & t \in (14.31, 32.03], \\ 0, & t \in (32.03, 32.76], \end{cases}$$

as shown in Fig. 5. Note that in this case, CAV  $i$  needs to start out by decelerating before entering the constrained arc.

*Safety-constrained optimal control with exit.* Assuming CAV  $k = 1$  enters the CZ at  $t_k^0 = 0$  with an initial speed  $v_k^0 = 10$  and exits at  $t_k^m = 41$  s with a terminal speed  $v_k^m = 10$  m/s, the optimal control is  $u_k^*(t) = 0.0017t - 0.0357$ . Then, we assume that CAV  $i = 2$  enters the CZ at  $t_i^0 = 1.5$  s with an initial speed  $v_i^0 = 12$  m/s, and the terminal time of CAV  $i$  is  $t_i^m = 42.5$  s

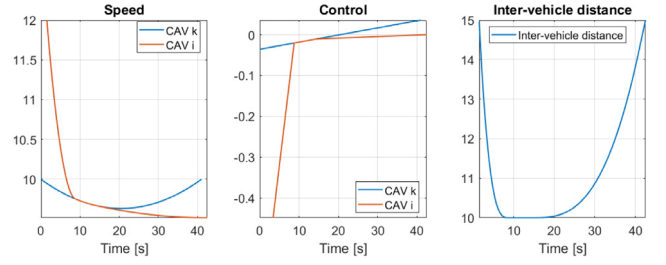


**Fig. 6.** The state constraint  $p_i(t) + \delta - p_k(t) \leq 0$  active (with entry and exit).

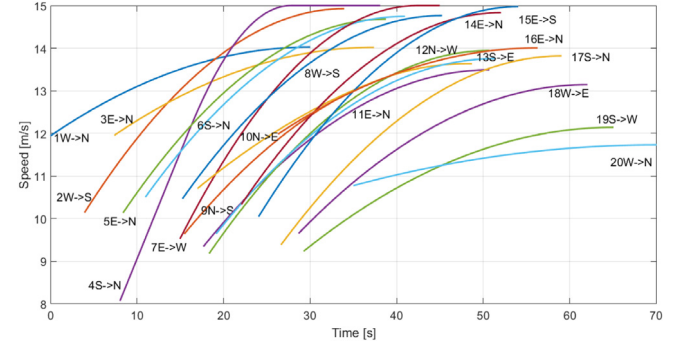


**Fig. 7.** Speed profiles of the first 20 CAVs in the CZ.

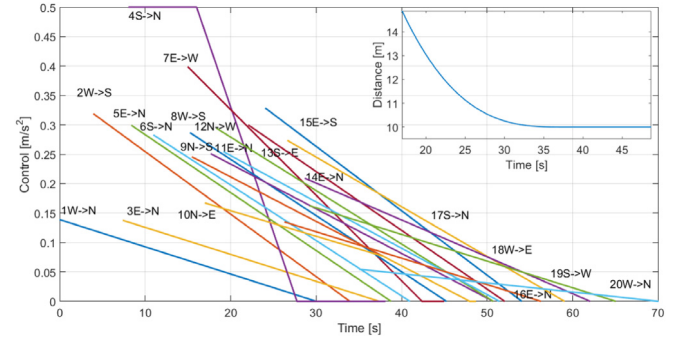


**Fig. 8.** Control input/acceleration profiles of the first 20 CAVs in the CZ.

satisfying  $t_i^m > t_k^m + \delta/v_k^m$  where the minimal safe following distance is  $\delta = 10$  m. The optimal control for CAV  $i$  is

$$u_i^*(t) = \begin{cases} 0.07971t - 0.7183, & t \in [1.5, 8.75] \\ 0.0017t - 0.0357, & t \in (8.75, 14.4), \\ 0.00038t - 0.0161 & t \in (14.4, 42.5), \end{cases}$$

as shown in Fig. 6.

### 5.1. Optimal trajectories in the CZ

The proposed decentralized optimal control framework inside the CZ is illustrated through simulation in MATLAB. We assumed a single lane for each traffic direction and the parameters used are:  $L = 400$  m,  $S = 30$  m; the speed constraints are  $v_{max} = 15$  m/s and  $v_{min} = 5$  m/s; the control constraints are  $u_{max} = 0.5$  m/s<sup>2</sup> and  $u_{min} = -0.5$  m/s<sup>2</sup>;  $S_L = \frac{3}{8}\pi S$ ,  $S_R = \frac{1}{8}\pi S$ ,  $\delta = 10$  m, and  $\Delta_i = 5, 3, 3$  s for a left turn, going straight, and a right turn respectively. CAVs arrive at the CZ based on a random arrival process which we assumed to be a Poisson process with rate  $\lambda = 1$  and the initial speeds are uniformly distributed over [8, 12] m/s.

The optimal speed and control trajectories in the CZ are shown in Figs. 7 and 8, with labels indicating the position of the CAV

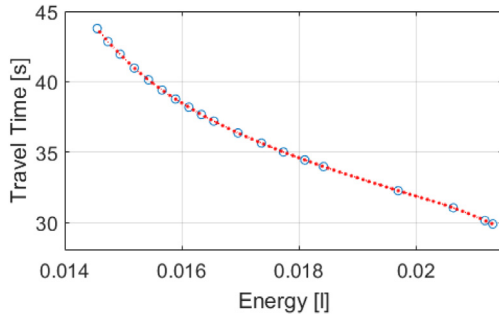


**Fig. 9.** Pareto efficiency sets and frontier corresponding to different combinations of energy consumption and traffic throughput in the CZ.

in the FIFO queue and the driving direction. To illustrate cases where the acceleration and speed constraints become active, note that for CAV #4, the optimal trajectory consists of three arcs: (i) a constrained arc starting at  $t_4^0 = 8.03$  s where the CAV accelerates at  $u_{max}$  until  $\tau_1 = 16.02$  s, (ii) an unconstrained arc where the CAV accelerates to  $v_{max}$  at  $\tau_2 = 27.57$  s, (iii) a constrained arc where the CAV cruises at  $v_{max}$  ( $u_i(t) = 0$ ) until it exits the CZ at  $t_4^m = 38.09$  s. For CAV #7, the optimal trajectory consists of two arcs: (i) an unconstrained arc starting at  $t_7^0 = 14.96$  s where the CAV keeps accelerating until it reaches  $v_{max}$  at  $\tau = 42.38$  s, (ii) a constrained arc where the CAV cruises at  $v_{max}$  ( $u_i(t) = 0$ ) until  $t_7^m = 44.96$  s.

To illustrate a case where the safety constraint is included, observe that CAV #10 is traveling on the same lane as #9. At  $\tau = 37.85$  s, #10 enters the constrained arc where  $p_{10}(t) + 10 - p_9(t) = 0$ . It then follows the optimal trajectory of #9, which can be reflected by the slope change in Fig. 8. The inter-vehicle distance between #9 and #10 is shown as a subfigure in Fig. 8. Observe that after #10 enters the constrained arc, it stays constrained until reaching the MZ without exiting. The lower bound of  $t_{10}^m$  happens to be constrained by #9, hence, once #10 enters the constrained arc, there is no incentive for it to exit.

The optimal solution to (22) varies as the weight  $\beta$  changes. To investigate the tradeoff between energy consumption and traffic throughput, we examine a range of cases with different  $\beta$  values and generate the associated Pareto sets illustrating the fact that no objective can be made better off without making at least one other objective worse. In (22), we use  $u_i^2(t)$  as a rough approximation of energy consumption, since it adequately captures its monotonic dependence on acceleration, while also allowing us to derive the analytical solution. However, to more accurately assess the impact of our controller, we use the polynomial metamodel proposed in Kamal, Mukai, Murata, and Kawabe (2013) which yields vehicle energy consumption in ml/s as a function of speed and acceleration:  $f = f_{cruise} + f_{accel}$  where  $f_{cruise} = w_0 + w_1 v_i(t) + w_2 v_i^2(t) + w_3 v_i^3(t)$  estimates the energy consumed by a vehicle cruising at a constant speed  $v_i(t)$ , and  $f_{accel} = u_i(t) \cdot [r_0 + r_1 v_i(t) + r_2 v_i^2(t)]$  estimates the additional energy consumed due to acceleration with  $u_i(t)$ . The polynomial coefficients  $w = [w_0, w_1, w_2, w_3]$  and  $r = [r_0, r_1, r_2]$  are calculated from experimental data. In addition, we use the average travel time inside the CZ, i.e.,  $t_i^m - t_i^0$  as a measurement of the traffic throughput. By obtaining all of the optimal solutions to (22) while varying the weight  $\beta$ , we can derive the Pareto sets and the Pareto frontier corresponding to different combinations of energy consumption and average travel time as shown in Fig. 9. Observe that there exists a tradeoff between minimizing energy consumption and maximizing traffic throughput.

To evaluate the effectiveness of the proposed solution, we carried out a comparison with the baseline scenario using VISSIM,

**Table 1**

Comparison with baseline scenario (signalized intersection).

	OC- $\beta_1$	OC- $\beta_2$	OC- $\beta_3$	Baseline
Travel time [s]	28.92	30.99	34.98	44.17
Energy [J]	0.047	0.045	0.042	0.052
OC Cost- $\beta_1$	11.42	/	/	16.57
OC Cost- $\beta_2$	/	4.08	/	5.52
OC Cost- $\beta_3$	/	/	1.50	1.84

$\beta_1 = 0.75$ ,  $\beta_2 = 0.5$ ,  $\beta_3 = 0.25$ .

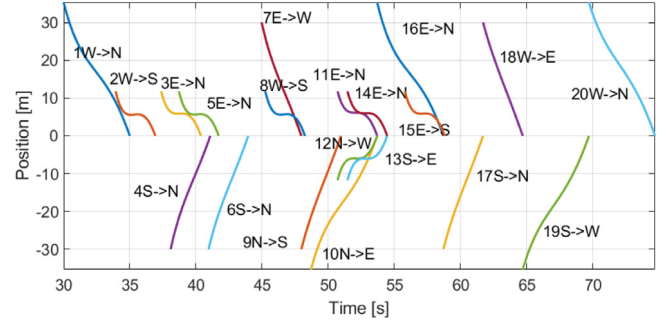


**Fig. 10.** Distance to the end of MZ of the first 20 CAVs in the MZ.

where all the vehicles are assumed to be non-CAVs under the control of traffic lights with fixed switching times. The comparison is shown in Table 1, where the weight  $\beta$  in (21), used for trading off energy and throughput, is set to 0.75, 0.5, and 0.25 respectively. When  $\beta = 0.5$  where energy and throughput are equally weighted, the energy consumption improvement is 13.46%, while the average travel time is improved by 29.84% compared to the baseline scenario. As  $\beta$  varies (see Table 1) the resulting tradeoff between travel time and energy changes as expected. Since our objective is to jointly minimize energy consumption and maximize traffic throughput, we also compute the value of the objective function in (21). As shown in Table 1, the optimized non-signalized performance is significantly better than the signalized baseline regardless of  $\beta$  values.

## 5.2. Optimal trajectories in the MZ

The proposed decentralized optimal control framework inside the MZ incorporating turns is illustrated through simulation in MATLAB with the same model parameters as in Section 5.1. The speeds at the entry of the MZ are the speeds at the end of the CZ, which are obtained from the optimal control problem formulated in the CZ. The speed at the exit of the MZ is set to  $v^f = 10$  m/s.

The position trajectories of the first 20 CAVs inside the MZ are shown in Fig. 10. CAVs are separated into two groups: those shown above zero are driving from east or west, and those below zero are driving from north or south, with labels indicating the position of the vehicles in the FIFO queue and the driving direction. Observe that CAV #11 belongs to  $\mathcal{O}_{12}(t)$  and no collision would occur between #11 and #12. Hence, they can be traveling inside the MZ at the same time, i.e.,  $t_{12}^f = t_{11}^f$ . Similarly, since CAV #12 belongs to  $\mathcal{O}_{13}(t)$ , no collision would occur between #12 and #13 as well. However, recalling the dependence of the terminal conditions on  $e, s, l, o$  in (18), #13 is constrained by #10 which may collide with it at the end of the MZ. As a result, #13 has to wait until #10 leaves the MZ for a distance  $\delta$ , which leads to  $t_{13}^f = t_{10}^f + \frac{\delta}{v_{10}^f}$ .

The optimal solution to (51) varies as the weight  $w$  changes. Similarly, to illustrate the tradeoff between passenger discomfort and energy consumption, we can examine a range of cases with



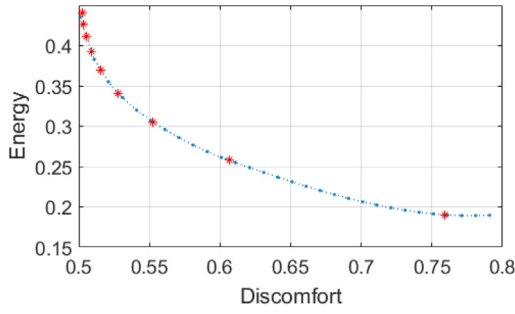


**Fig. 11.** Pareto efficiency sets and frontier corresponding to different combinations of energy consumption and passenger discomfort in the MZ.

different weights and generate the associated Pareto sets. In Fig. 11, we use  $u_i^2(t)$  and  $J_i^2(t)$  as rough approximations of energy consumption and passenger discomfort respectively. Clearly, there is a tradeoff between these two metrics as the vehicle turns within the intersection.

Compared to MATLAB, the use of the VISSIM simulation platform allows us to test our approach under more realistic conditions. Under such conditions and despite the presence of errors and delays, we have shown that our decentralized optimal control framework is able to outperform a baseline scenario in terms of both energy consumption and travel time. In addition, we are pursuing field tests using an actual CAV in Mcity, a test bed located at the University of Michigan North Campus in Ann Arbor, Michigan, where realistic V2V and V2I communication conditions are also included.

## 6. Conclusions and future work

We have extended earlier work in Malikopoulos et al. (2018) and Zhang et al. (2016) where a decentralized optimal control framework was established for optimally controlling CAVs crossing an urban intersection without considering turns. In this paper, we have included left and right turns and considered a new optimal control problem formulation where the tradeoff between energy and travel time is explicitly quantified for CAVs in the CZ and all safety constraints are incorporated. Despite the added complexity of turns, we have shown that the optimal solution can still be obtained in decentralized fashion, with each CAV requiring information from a subset of other CAVs. This enables the on-line solution to be obtained by on-board computation resources for each individual CAV. In addition, we have formulated another optimization problem with the objective of minimizing passenger discomfort while the vehicle turns at the MZ of the intersection, and investigated the tradeoff between minimizing energy consumption and passenger discomfort.

Clearly, our analysis provides an optimal *planned* trajectory which should be viewed as a reference to be tracked by a lower-level CAV controller, for example using Model Predictive Control (MPC) methods. In fact, we have found that an approach based on Control Barrier Functions (CBFs) (Xiao, Belta, & Cassandras, 2019) is preferable to MPC. This approach is similar in spirit to MPC, but can handle nonlinearities in the vehicle dynamics, noise in the process and measurements, and more complex objective functions than our optimal control formulation in (21), while also possessing a “forward invariance” property in guaranteeing that all constraints are not violated.

Ongoing research is exploring the effect of partial CAV penetration in mixed traffic situations where both CAVs and human-driven vehicles share the road (Zhang & Cassandras, 2018b, 2019a). When the CAV is constrained by a preceding non-CAV, the

CAV will enter an “adaptive following” mode where it proceeds in an energy-optimal way while adaptively maintaining a safe following distance from the preceding non-CAV.

Since the focus of this paper is on the constrained optimization of vehicle trajectories, the impact of the communication infrastructure is not explicitly addressed here, but is a topic of ongoing research. The precise nature of such an infrastructure supporting CAV connectivity is obviously a critical factor in the implementation of our decentralized optimal control framework. In a parallel effort (Zhang, Cassandras, Li, & Mosterman, 2019), we conducted several simulation studies based on real-world transportation systems including an investigation of the impact of communication delays on vehicle safety where we found that a large delay could lead to potential rear-end collisions. We also note that we have made the assumption that all vehicles are equipped with on-board sensors so that, even with the presence of communication delays, the vehicles are able to avoid collisions should an emergency arise. In particular, if the communication is not reliable, then we have to forgo optimality and revert control back to the driver to ensure safety.

Future work will investigate more complicated safety constraints (Zhang & Cassandras, 2019b) as well as the coupling between multiple intersections, and the possibility of extending the rescheduling approach in Zhang and Cassandras (2018a) to potentially improve overall traffic throughput.

## Appendix A. Constrained optimal control analysis

In this Appendix, we discuss the effect of the control and state constraints not included in our analysis of Section 3.2. Clearly, there are a number of possible situations that may arise, including the possibility of both the state constraint  $v_i(t) - v_{max} \leq 0$  and the control constraint  $u_i(t) - u_{max} \leq 0$  becoming active (e.g., CAV #4 in Figs. 7 and 8). The analysis provided here is limited to the state constraint  $v_i(t) - v_{max} \leq 0$  or the control constraint  $u_i(t) - u_{max} \leq 0$  each becoming active on its own. These basic cases serve as “building blocks” to handle situations of multiple constraints becoming active when this is feasible.

### A.1. State constraint $v_i(t) - v_{max} \leq 0$ active only

When the state constraint  $v_i(t) - v_{max} \leq 0$  becomes active at  $\tau$ , the jump conditions in (45) become

$$\begin{aligned} \lambda_i^p(\tau^-) &= \lambda_i^p(\tau^+) + \pi_i^p \frac{\partial(v_i(\tau) - v_{max})}{\partial p_i} = \lambda_i^p(\tau^+), \\ \lambda_i^v(\tau^-) &= \lambda_i^v(\tau^+) + \pi_i^v \frac{\partial(v_i(\tau) - v_{max})}{\partial v_i} \\ &= \lambda_i^v(\tau^+) + \pi_i^v(\tau), \\ H_i(\tau^-) &= H_i(\tau^+) - \pi_i(v_i(\tau) - v_{max})_t = H_i(\tau^+), \\ \pi_i(v_i(\tau) - v_{max}) &= 0, \pi_i \geq 0. \end{aligned} \quad (64)$$

Thus, we have  $H_i(\tau^-) = H_i(\tau^+)$  and  $\lambda_i^p(\tau^-) = \lambda_i^p(\tau^+)$ . Based on this fact, we have the following result whose proof is similar to that of Theorem 3.

**Theorem 5.** *The optimal control  $u_i(t)$  is continuous at the junction  $\tau$  of the unconstrained and  $v_{max}$ -constrained arcs, i.e.,  $u_i^*(\tau^-) = u_i^*(\tau^+)$ .*

For this case, CAV  $i$  remains on the constrained arc until it reaches the MZ and we have

$$u_i(t) = \begin{cases} a_i t + b_i, & t \leq \tau, \\ 0, & t > \tau. \end{cases} \quad (65)$$

where  $\tau$  is the entry point of the constrained arc  $v_i(t) - v_{max} = 0$ , and, due to Theorem 5, we also have  $a_i \tau + b_i = 0$ .

Combined with the boundary conditions and the transversality conditions (33), we have the following conditions

$$\frac{1}{6}a_i \cdot (t_i^0)^3 + \frac{1}{2}b_i \cdot (t_i^0)^2 + c_i t_i^0 + d_i = 0 \quad (66a)$$

$$\frac{1}{2}a_i \cdot (t_i^0)^2 + b_i t_i^0 + c_i = v_i^0 \quad (66b)$$

$$\frac{1}{6}a_i \tau^3 + \frac{1}{2}b_i \tau^2 + c_i \tau + d_i - L - v_{\max}(t_i^m - \tau) = 0 \quad (66c)$$

$$\frac{1}{2}a_i \tau^2 + b_i \tau + c_i = v_{\max} \quad (66d)$$

$$a_i \tau + b_i = 0 \quad (66e)$$

$$\gamma + a_i \cdot v_{\max} = 0 \quad (66f)$$

where  $a_i$ ,  $b_i$ ,  $c_i$ ,  $d_i$ ,  $\tau$  and  $t_i^m$  are obtained by solving these six equations. The first two immediately follow from the initial conditions, while (66c) follows from  $p_i(\tau) + v_{\max} \cdot (t_i^m - \tau) = L$ , (66d) follows from  $v_i(\tau) = v_{\max}$ , and (66e) follows from the fact that  $u_i(\tau^-) = u_i(\tau^+) = 0$ . The last Eq. (66f) follows from the continuity of the Hamiltonian and the transversality condition  $H_i(t_i^m) = 0$ . Note that in this case we assumed a free terminal time  $t_i^m$ . If  $t_i^m$  is fixed, then we simply remove the transversality condition (66f). Simulation example of this case arises in Figs. 7 and 8, e.g., CAV #7.

#### A.2. Control constraint $u_i(t) - u_{\max} \leq 0$ active only

When the control constraint  $u_i(t) - u_{\max} \leq 0$  is active at  $\tau$ , both the Hamiltonian and the costates are continuous according to (45). For this case, we have

$$u_i(t) = \begin{cases} u_{\max}, & t \leq \tau, \\ a_i t + b_i, & t > \tau. \end{cases} \quad (67)$$

Combined with the boundary conditions and the transversality conditions (33), we have the following conditions

$$(\tau - t_i^0)[v_i^0 + \frac{1}{2}u_{\max}(\tau - t_i^0)] - (\frac{1}{6}a_i \tau^3 + \frac{1}{2}b_i \tau^2 + c_i \tau + d_i) = 0 \quad (68a)$$

$$v_i^0 + u_{\max}(\tau - t_i^0) - (\frac{1}{2}a_i \tau^2 + b_i \tau + c_i) = 0 \quad (68b)$$

$$a_i \tau + b_i = u_{\max} \quad (68c)$$

$$\frac{1}{6}a_i \cdot (t_i^m)^3 + \frac{1}{2}b_i \cdot (t_i^m)^2 + c_i t_i^m + d_i = L \quad (68d)$$

$$a_i t_i^m + b_i = 0 \quad (68e)$$

$$\gamma - \frac{1}{2}b_i^2 + a_i c_i = 0 \quad (68f)$$

where  $a_i$ ,  $b_i$ ,  $c_i$ ,  $d_i$ ,  $\tau$  and  $t_i^m$  are obtained by solving these equations. The first two equations (68a) and (68b) follow from the fact that  $p_i(\tau^-) = p_i(\tau^+)$  and  $v_i(\tau^-) = v_i(\tau^+)$ , (68c) follows from the fact that  $u_i(\tau^-) = u_i(\tau^+) = u_{\max}$ , (68d) follows from the terminal condition, and the last two equations follow from the transversality conditions. In this case, we assume a free terminal time  $t_i^m$ . If  $t_i^m$  is fixed, then we simply remove the last transversality condition (68f).

#### Appendix B. Proof of lemmas

**Lemma 1.** For the unconstrained problem with free terminal time, the optimal control is non-negative, i.e.,  $u_i^*(t) \geq 0$ , and monotonically non-increasing.

**Proof.** To prove that  $u_i^*(t) \geq 0$ , let us assume that the optimal control includes an interval that is negative, i.e.,  $u_i^*(t) < 0$  for  $t \in [t_1, t_2]$ , and  $u_i^*(t) \geq 0$  for  $t \in [t_i^0, t_1] \cup [t_2, t_i^m]$ . Next, we construct another control  $u_i^c(t)$  which is the same as  $u_i^*(t)$  except that  $u_i^c(t) = 0$  for  $t \in [t_1, t_2]$ . Let us first prove that  $u_i^c(t)$  is feasible. Note that  $u_i^c(t) = u_i^*(t)$  for  $t \in [t_i^0, t_1] \cup [t_2, t_i^m]$ , hence,  $u_i^c(t)$  must be feasible for  $t \in [t_i^0, t_1]$ . Moreover, for  $t \in [t_1, t_2]$ ,  $u_i^c(t) = 0$  does not violate any control constraints. In addition, since we have  $v_{\min} < v_i^c(t_1) < v_{\max}$  and  $u_i^c(t) = 0$  for  $t \in [t_1, t_2]$ , it follows that  $v_i^c(t) = v_i(t_1)$  and  $v_{\min} < v_i^c(t) < v_{\max}$  for  $t \in [t_1, t_2]$ . Hence, the speed constraints are satisfied as well. By assumption, the safety constraint (3) is inactive over  $[t_i^0, t_1]$ . If, under  $u_i^c(t)$ , the safety constraint remains inactive over  $[t_1, t_2]$ , then  $u_i^c(t)$  is feasible. Otherwise, since (3) is inactive under  $u_i^*(t)$ , there exists some  $\epsilon > 0$  such that it remains inactive over  $[t_1, t_1 + \epsilon]$ , in which case we modify  $u_i^c(t)$  so that  $u_i^c(t) = 0$  for  $t \in [t_1, t_1 + \epsilon]$  and  $u_i^c(t) = u_i^*(t)$  for  $t \in (t_1 + \epsilon, t_2]$  which ensures  $u_i^c(t)$  is feasible over  $[t_1, t_2]$ . Next, since  $u_i^*(t) < 0$  and  $u_i^c(t) = 0$  for  $t \in [t_1, t_1 + \epsilon]$ , we have  $v_i^*(t) < v_i^c(t)$  for  $t \in [t_1, t_2]$  and for  $t \in [t_2, t_i^m]$ . This implies that it is possible that  $v_i^c(t_3) = v_{\max}$  for some  $t_3 \in (t_2, t_i^m]$ . If that happens, then we modify  $u_i^c(t)$  so that  $u_i^c(t) = 0$ , hence  $v_i^c(t) = v_{\max}$ , for  $t \in [t_3, t_i^m]$  and  $u_i^c(t)$  is feasible over all  $t \in [t_i^0, t_i^m]$ . Since  $v_i^*(t) < v_i^c(t)$  for  $t \in [t_1, t_2]$  and  $v_i^*(t) \leq v_i^c(t)$  for  $t \in [t_i^0, t_i^m]$ , it follows that  $t_i^{m*} > t_i^{mc}$ , or  $t_i^{m*} - t_i^0 > t_i^{mc} - t_i^0$ , which indicates that the optimal control  $u_i^*(t)$  leads to a longer travel time compared to  $u_i^c(t)$ . Denoting the energy consumption in (22) as  $J_u(u_i(t))$  and allowing for the possibility that there exists  $t_3$  such that  $t_2 < t_3 \leq t_i^m$  (otherwise,  $t_3 = t_i^m$ ), we have

$$\begin{aligned} J_u(u_i^*(t)) &= \int_{t_i^0}^{t_1} \frac{1}{2}(u_i^*)^2 dt + \int_{t_1}^{t_2} \frac{1}{2}(u_i^*)^2 dt \\ &\quad + \int_{t_2}^{t_3} \frac{1}{2}(u_i^*)^2 dt + \int_{t_3}^{t_i^m} \frac{1}{2}(u_i^*)^2 dt \\ &> \int_{t_i^0}^{t_1} \frac{1}{2}(u_i^*)^2 dt + \int_{t_2}^{t_3} \frac{1}{2}(u_i^*)^2 dt = J_u(u_i^c(t)) \end{aligned}$$

where we have used the fact that  $u_i^c(t) = 0$  for at least  $t \in [t_1, t_1 + \epsilon]$  and  $u_i^c(t) = u_i^*(t)$  for  $t \in [t_i^0, t_1] \cup [t_2, t_3]$ . In view of the objective function (21), since we have shown that  $t_i^{m*} - t_i^0 > t_i^c - t_i^0$  and  $J_u(u_i^*(t)) > J_u(u_i^c(t))$ , we can see that the optimal control  $u_i^*(t)$  incurs a larger cost compared to  $u_i^c(t)$ , which contradicts the assumption that  $u_i^*(t)$  is the optimal control. Therefore,  $u_i^*(t)$  cannot be negative at any  $t \in [t_i^0, t_i^m]$  and we have  $u_i^*(t) \geq 0$  as long as the optimal trajectory is unconstrained.

To prove that  $u_i^*(t)$  is monotonically non-increasing, observe that  $u_i^*(t_i^m) = 0$  from (41d). Since the optimal control is a linear function of time as indicated by (38) and non-negative as established above, it follows that  $u_i^*(t)$  is monotonically non-increasing. ■

**Lemma 2.** For the unconstrained problem with free terminal time, it is not possible for constraints  $v_{\min} - v_i(t) \leq 0$  and/or  $u_{\min} - u_i(t) \leq 0$  to become active.

**Proof.** By Lemma 1,  $u_i^*(t) \geq 0$ . Hence,  $u_{\min} - u_i(t) \leq 0$  cannot become active. Since, by assumption,  $v_{\min} < v_i^0 < v_{\max}$ ,  $v_i^*(t)$  cannot reach  $v_{\min}$  and the constraint  $v_{\min} - v_i(t) \leq 0$  cannot become active. ■

**Lemma 3.** For the unconstrained problem with fixed terminal time, the optimal control must be either monotonically non-increasing and  $u_i^*(t) \geq 0$ , or monotonically non-decreasing and  $u_i^*(t) \leq 0$ .

**Proof.** Due to the linearity of the unconstrained optimal control in (38),  $u_i^*(t)$  must be either non-increasing or non-decreasing over all  $t \in [t_i^0, t_i^m]$ . With the terminal time fixed, the last equation in (42) gives  $u_i^*(t_i^m) = 0$ . Therefore, when  $u_i^*(t)$  is monotonically non-increasing, we have  $u_i^*(t) \geq 0$ ; when  $u_i^*(t)$  is monotonically non-decreasing, we have  $u_i^*(t) \leq 0$ . ■

## References

- Aashto, A. (2001). Policy on geometric design of highways and streets. In *American association of state highway and transportation officials*, vol. 1, no. 990 (p. 158). Washington, DC.
- Athans, M. (1969). A unified approach to the vehicle-merging problem. *Transportation Research*, 3(1), 123–133.
- Bryson, A., & Ho, Y.-C. (1975). *Applied optimal control: Optimization, estimation, and control (revised edition)*. Levittown, Pennsylvania: Taylor & Francis.
- de La Fortelle, A. (2010). Analysis of reservation algorithms for cooperative planning at intersections. In *13th international IEEE conference on intelligent transportation systems* (pp. 445–449).
- Dresner, K., & Stone, P. (2004). Multiagent traffic management: a reservation-based intersection control mechanism. In *Proceedings of the third international joint conference on autonomous agents and multiagents systems* (pp. 530–537).
- Dresner, K., & Stone, P. (2005). Multiagent traffic management: An improved intersection control mechanism. In *Proceedings of the fourth international joint conference on autonomous agents and multiagent systems* (pp. 471–477). ACM.
- Dresner, K., & Stone, P. (2008). A multiagent approach to autonomous intersection management. *Journal of Artificial Intelligence Research*, 31, 591–653.
- Fleck, J. L., Cassandras, C. G., & Geng, Y. (2016). Adaptive quasi-dynamic traffic light control. *IEEE Transactions on Control Systems Technology*, 24(3), 830–842.
- Gilbert, E. G. (1976). Vehicle cruise: Improved fuel economy by periodic control. *Automatica*, 12(2), 159–166.
- Hellström, E., Åslund, J., & Nielsen, L. (2010). Design of an efficient algorithm for fuel-optimal look-ahead control. *Control Engineering Practice*, 18(11), 1318–1327.
- Hogan, N. (1984). Adaptive control of mechanical impedance by coactivation of antagonist muscles. *IEEE Transactions on Automatic Control*, 29(8), 681–690.
- Hooker, J. (1988). Optimal driving for single-vehicle fuel economy. *Transportation Research Part A: General*, 22(3), 183–201.
- Huang, S., Sadek, A., & Zhao, Y. (2012). Assessing the mobility and environmental benefits of reservation-based intelligent intersections using an integrated simulator. *IEEE Transactions on Intelligent Transportation Systems*, 13(3), 1201–1214.
- Kamal, M., Mukai, M., Murata, J., & Kawabe, T. (2013). Model predictive control of vehicles on urban roads for improved fuel economy. *IEEE Transactions on Control Systems Technology*, 21(3), 831–841.
- Kim, K.-D., & Kumar, P. R. (2014). An MPC-based approach to provable system-wide safety and liveness of autonomous ground traffic. *IEEE Transactions on Automatic Control*, 59(12), 3341–3356.
- Lee, J., & Park, B. (2012). Development and evaluation of a cooperative vehicle intersection control algorithm under the connected vehicles environment. *IEEE Transactions on Intelligent Transportation Systems*, 13(1), 81–90.
- Levine, W., & Athans, M. (1966). On the optimal error regulation of a string of moving vehicles. *IEEE Transactions on Automatic Control*, 11(3), 355–361.
- Li, S. E., Peng, H., Li, K., & Wang, J. (2012). Minimum fuel control strategy in automated car-following scenarios. *IEEE Transactions on Vehicular Technology*, 61(3), 998–1007.
- Li, L., & Wang, F.-Y. (2006). Cooperative driving at blind crossings using intervehicle communication. *IEEE Transactions in Vehicular Technology*, 55(6), 1712–1724.
- Malikopoulos, A., & Aguilar, J. (2013). An optimization framework for driver feedback systems. *IEEE Transactions on Intelligent Transportation Systems*, 14(2), 955–964.
- Malikopoulos, A. A., Cassandras, C. G., & Zhang, Y. J. (2018). A decentralized energy-optimal control framework for connected automated vehicles at signal-free intersections. *Automatica*, 93, 244–256.
- Margiotta, R., & Snyder, D. An agency guide on how to establish localized congestion mitigation programs. U.S. Department of Transportation. Federal Highway Administration, Tech. Rep., 2011.
- Miculescu, D., & Karaman, S. (2014). Polling-systems-based control of high-performance provably-safe autonomous intersections. In *53rd IEEE conference on decision and control*.
- Ntousakis, I. A., Nikolas, I. K., & Papageorgiou, M. (2016). Optimal vehicle trajectory planning in the context of cooperative merging on highways. *Transportation Research Part C: Emerging Technologies*, 71, 464–488.
- Rajamani, R., Tan, H.-S., Law, B. K., & Zhang, W.-B. (2000). Demonstration of integrated longitudinal and lateral control for the operation of automated vehicles in platoons. *IEEE Transactions on Control Systems Technology*, 8(4), 695–708.
- Rios-Torres, J., & Malikopoulos, A. A. (2017). A survey on the coordination of connected and automated vehicles at intersections and merging at highway on-ramps. *IEEE Transactions on Intelligent Transportation Systems*, 18(5), 1066–1077.
- SAE international SAE international, Taxonomy and definitions for terms related to driving automation systems for on-road motor vehicles, SAE International, (J3016).
- Schrank, D., Eisele, B., Lomax, T., & Bak, J. (2015). *Urban Mobility Scorecard*. Texas A&M Transportation Institute, INRIX, Inc. <http://static.tti.tamu.edu/tti.tamu.edu/documents/mobility-scorecard-2015.pdf>.
- Shladover, S. E., Desoer, C. A., Hedrick, J. K., Tomizuka, M., Walrand, J., Zhang, W.-B., McMahon, D. H., Peng, H., Sheikholeslam, S., & McKeown, N. (1991). Automated vehicle control developments in the PATH program. *IEEE Transactions on Vehicular Technology*, 40(1), 114–130.
- Tachet, R., Santi, P., Sobolevsky, S., Reyes-Castro, L. I., Frazzoli, E., Helbing, D., & Ratti, C. (2016). Revisiting street intersections using slot-based systems. *PLoS one*, 11(3), e0149607.
- Varaiya, P. (1993). Smart cars on smart roads: problems of control. *IEEE Transactions on Automatic Control*, 38(2), 195–207.
- Xiao, W., Belta, C., & Cassandras, C. (2019). Decentralized optimal merging at an intersection: a control barrier function approach. In *10th ACM/IEEE international conference on cyber-physical systems* (pp. 270–279).
- Yan, F., Dridi, M., & El Moudni, A. (2009). Autonomous vehicle sequencing algorithm at isolated intersections. In *2009 12th international IEEE conference on intelligent transportation systems* (pp. 1–6).
- Zhang, Y., & Cassandras, C. G. (2018a). A decentralized optimal control framework for connected automated vehicles at urban intersections with dynamic resequencing. In *57th IEEE conference on decision and control* (pp. 217–222).
- Zhang, Y., & Cassandras, C. G. (2018b). The penetration effect of connected automated vehicles in urban traffic: an energy impact study. In *2nd IEEE conference on control technology and applications* (pp. 620–625).
- Zhang, Y., & Cassandras, C. G. (2019a). An impact study of integrating connected automated vehicles with conventional traffic. *Annual Reviews in Control*.
- Zhang, Y., & Cassandras, C. G. (2019b). Joint time and energy-optimal control of connected automated vehicles at signal-free intersections with speed-dependent safety guarantees. In *58th IEEE conference on decision and control*. to appear.
- Zhang, Y., Cassandras, C. G., Li, W., & Mosterman, P. J. (2019). A discrete-event and hybrid traffic simulation model based on SimEvents for intelligent transportation system analysis in Mcity. *Discrete Event Dynamic Systems*, 1–31.
- Zhang, Y., Cassandras, C. G., & Malikopoulos, A. A. (2017). Optimal control of connected automated vehicles at urban traffic intersections: A feasibility enforcement analysis. In *Proceedings of the 2017 American control conference* (pp. 3548–3553).
- Zhang, Y., Malikopoulos, A. A., & Cassandras, C. G. (2016). Optimal control and coordination of connected and automated vehicles at urban traffic intersections. In *Proceedings of the American control conference* (pp. 6227–6232).
- Zhu, F., & Ukkusuri, S. V. (2015). A linear programming formulation for autonomous intersection control within a dynamic traffic assignment and connected vehicle environment. *Transportation Research Part C: Emerging Technologies*.
- Zohdy, I. H., Kamalanathsharma, R. K., & Rakha, H. (2012). Intersection management for autonomous vehicles using iCACC. In *2012 15th international IEEE conference on intelligent transportation systems* (pp. 1109–1114).



**Yue Zhang** received the B.S. degree in Electronics and Information Engineering from Huazhong University of Science and Technology, Wuhan, China in 2013. She is currently pursuing the Ph.D. degree with the Division of Systems Engineering and the Center for Information and Systems Engineering (CISE) at Boston University, working with Prof. Christos G. Cassandras. Her research interests include control and optimization of hybrid systems and big data analytics, with applications to intelligent transportation systems. During the summer of 2015, she worked as a research intern with the National Transportation Research Center at the Oak Ridge National Laboratory, Oak Ridge, TN. During the summer of 2018, she worked as a software development intern at Facebook, Menlo Park, CA. During the summer of 2019, she interned with the Autonomous Vehicles team at NVIDIA, Santa Clara, CA.



**Christos G. Cassandras** is Distinguished Professor of Engineering at Boston University. He is Head of the Division of Systems Engineering, Professor of Electrical and Computer Engineering, and co-founder of Boston University's Center for Information and Systems Engineering (CISE). He received degrees from Yale University, Stanford University, and Harvard University. In 1982–84 he was with ITP Boston, Inc. where he worked on the design of automated manufacturing systems. In 1984–1996 he was a faculty member at the Department of Electrical and Computer Engineering,

University of Massachusetts/Amherst. He specializes in the areas of discrete event and hybrid systems, cooperative control, stochastic optimization, and computer simulation, with applications to computer and sensor networks, manufacturing systems, and transportation systems. He has published about 400 refereed papers in these areas, and six books. He has guest-edited several technical journal issues and currently serves on several journal Editorial Boards, including Editor of *Automatica*. In addition to his academic activities, he has worked extensively with industrial organizations on various systems integration projects and the development of decision support software. He has most recently collaborated with The MathWorks, Inc. in the development of the discrete event

and hybrid system simulator SimEvents.

Dr. Cassandras was Editor-in-Chief of the *IEEE Transactions on Automatic Control* from 1998 through 2009 and has also served as Editor for *Technical Notes and Correspondence* and Associate Editor. He was the 2012 President of the IEEE Control Systems Society (CSS). He has also served as Vice President for Publications and on the Board of Governors of the CSS, as well as on several IEEE committees, and has chaired several conferences. He has been a plenary/keynote speaker at numerous international conferences, including the 2017 IFAC World Congress, the American Control Conference in 2001 and the IEEE Conference on Decision and Control in 2002 and 2016, and has also been an IEEE Distinguished Lecturer.

He is the recipient of several awards, including the 2011 IEEE Control Systems Technology Award, the Distinguished Member Award of the IEEE Control Systems Society (2006), the 1999 Harold Chestnut Prize (IFAC Best Control Engineering Textbook) for *Discrete Event Systems: Modeling and Performance Analysis*, a 2011 prize and a 2014 prize for the IBM/IEEE Smarter Planet Challenge competition, the 2014 Engineering Distinguished Scholar Award at Boston University, several honorary professorships, a 1991 Lilly Fellowship and a 2012 Kern Fellowship. He is a member of Phi Beta Kappa and Tau Beta Pi. He is also a Fellow of the IEEE and a Fellow of the IFAC.